Final Technical Report
Reporting Period: September 1, 2012 to August 31, 2015
Date of Submission of Report: February 29, 2015

Federal Agency/ Organization Element: DOE/EERE/ Office of Advanced Manufacturing Program (AMO)

Award Number: DE-EE0005761

Project Title: A New Method for Low Cost Production of Titanium Alloys for Reducing Energy Consumption of Mechanical Systems

Project Period: 09/01/2012 through 02/15/2016

Recipient Organization:
UNIVERSITY OF UTAH, THE
Attn: GARY CHRISTENSEN
75 SOUTH 2000 EAST, 2ND FLOOR
SALT LAKE CITY UT 841128930

DUNS Number: 009095365

Principal Investigator: Z. Zak Fang
801-581-8128
zak.fang@utah.edu

Co-PI: Ravi Chandran
801-587-7197
ravi.chandran@utah.edu

Senior Staff: Mark Koopman
205.789.2042
mark.koopman@utah.edu

Business Contact: Jesse Pugh, jesse.pugh@osp.utah.edu, (801) 581-3008

Partners: Reading Alloys / Ametek Inc.
Joe Capone joe.capone@ametek.com, (724) 575-0358

DOE Technology Manager:	Stephen Sikrica	Stephen.Sikirica@ee.doe.gov, (202) 586-5041
DOE Project Officer:	Gibson Asuquo	Gibson.Asuquo@go.doe.gov, (720) 356-1433
DOE Project Monitor:	Kristen McDaniel	Kristen.McDaniel@go.doe.gov, (720) 356-1285
DOE Contract Specialist:	Melissa Jacobi	Melissa.jacobi@go.doe.gov, (720) 356-1658
DOE Contract Officer:	Kristen Cadigan	Kristen.Cadigan@ee.doe.gov, (720) 356-1789

Submitting Official: Z. Zak Fang, Professor, PI
Tel. (801) 581-8128
Email: zak.fang@utah.edu

Signature of Submitting Official: Z. Zak Fang

Acknowledgment: This report is based upon work supported by the U. S. Department of Energy under Award No. DE-EE0005761

Disclaimer:

Table of Contents

List of Acronyms

BE – blended element (in reference to powder metallurgy methods)
CIP – cold isostatic pressing
GFM – gyratory forging machine
GHG – greenhouse gas
HCF – high cycle fatigue
HIP – hot isostatic pressing
HMO – heavy mineral oil
HSPT – hydrogen sintering and phase transformations
LCF – low cycle fatigue
LMO – light mineral oil
PA – prealloyed (in reference to powder metallurgy methods)
PIF – pneumatic isostatic forging
PM – powder metallurgy
SEM – scanning electron microscope
SS – stainless steel
TGA – thermogravimetric analysis
UTS – ultimate tensile strength
VAR – vacuum arc remelting
YS – yield strength

List of Tables

List of Figures

Appendices

Executive Summary

This project investigated an innovative manufacturing process intended to minimize the cost of production of titanium materials and components, and increase the adoption of Ti components for energy consuming applications, such as automobiles. A key innovation of the proposed manufacturing approach is a novel Ti powder sintering technology for making titanium materials with ultrafine grain microstructure in the as-sintered state with minimum, or an absence, of post-sintering processes. The new sintering technology is termed Hydrogen Sintering and Phase Transformations (HSPT), and constitutes a promising manufacturing technology that can be used to produce titanium (Ti) materials and components in a near-net-shape form, thus also minimizing machining costs. Our objective was to meet, or possibly surpass, the mechanical property levels for ASTM B348 Grade 5 for wrought Ti-6Al-4V. Although specific applications call for varying mechanical property requirements, ASTM B348 was created for the demanding applications of the aerospace industry, and is the established standard for Ti-6Al-4V. While the primary goal was to meet, or exceed this standard, the team also had the goal of demonstrating this could be done at a significantly lower cost of production.

Interim goals of the project were to fully develop this novel sintering process, and provide sufficient baseline testing to make the method practical and attractive to industry. By optimizing the process parameters for the sintering of titanium hydride (TiH_2) powders in a hydrogen atmosphere and controlling the phase transformations during and after sintering, the HSPT process was expected to reduce the energy consumption, and thus cost, of making Ti alloys and fabricating Ti components. The process was designed such that no high temperature melting is required for producing Ti alloys; little or no post-sintering processing is needed for producing desired microstructures (and therefore enhanced mechanical properties), and finally, minimum machining is needed to fabricate finished Ti components. An energy analysis within this report provides more detail, but calculated values indicate that the HSPT process is less than half as energy intensive as conventional wrought processing, while producing mechanical properties that are comparable.

In addition to the energy savings anticipated from the industrial production of Ti components, a second prong of energy savings resides in the use phase of components produced, primarily from use in the transportation sector. Titanium has a number of material qualities appropriate for the auto industry, particularly low mass and corrosion resistance. By reducing the weight of automobiles and other vehicles, energy costs and CO_2 production will be reduced over the lifetime of the vehicles, and components in corrosive environments on vehicles, such as exhaust systems and other under carriage parts, may not have to be replaced during a vehicle's lifetime. Our analysis indicates that by replacing only 5.6 kg of steel parts in an auto with Ti components across the entire US fleet would save approximately 486 million gallons of gasoline per year. This correlates to a reduction of 3.6 million metric tons of CO_2 per year. The potential for replacing many more of the steel parts in automobiles with lighter weight titanium components is clear.

The project was very successful overall, meeting all milestones and surpassing project goals in terms of mechanical properties and microstructures produced. In addition to tensile properties, fatigue properties were emphasized in the project work. Powder metallurgy processes often have porosity to some degree in their final microstructure, and porosity is a well-known cause of crack initiation and low fatigue performance. Although many automobile applications do not undergo fatigue stress regimes, many others do encounter cyclic stress, and design criteria

in the latter case require good fatigue properties. Production and testing of HSPT parts showed excellent tensile properties and fracture toughness, and fatigue properties that exceeded all previously reported powder metallurgy Ti methods, overlapping with wrought processed values. Fatigue limits exceeded 500 MPa and tensile strength exceeded 1,000 MPa while maintaining good ductility.

Microstructures produced during the project period easily surpassed pre-project expectations. In addition to producing very fine grains in the as-sintered state (without post sintered thermo-mechanical work), porosity was reduced and industrially relevant microstructures previously undemonstrated in any other powder metallurgy titanium method were produced using HSPT materials. These microstructures, both bi-modal and globularized, were produced with simple post-sinter heat treatments, but without the need for energy intensive mechanical work. The employed heat treatments expanded the available mechanical property range (tensile strength vs. ductility) of the HSPT system in Ti-6Al-4V.

The project has resulted in the publication, thus far, of five refereed journal articles and five conference proceedings papers, as well as a patent application, two dissertations and a master's thesis. Two additional journal articles are currently under review, and at least three others are currently in preparation, with several additional students anticipated to graduate within the coming year. Presentations and papers were a particular focus of the second half of the project, once significant experimentation had been performed and analyzed. As part of our efforts to disseminate information of our results, the Ti research teams within Prof. Fang's and Prof. Chandran's research groups had a strong presence at the 13th World Conference on Ti, August 16-20, 2015, in San Diego. Several research groups in the US and in Europe are now performing experiments using the HSPT process.

Accompanying efforts to bring HSPT to the Ti community at large, and industry in particular, work has continued with our partners and with other interested industrial Ti users and producers, including Boeing and GKN (a major powder metallurgy parts manufacturer). Commercialization has been a central focus of the final phase of the project, and Reading Alloys signed a provisional licensing agreement in summer of 2015. They are currently seeking an appropriate customer with which to pursue initial parts manufacturing efforts. Other licensing options and partners are continuing to be pursued.

The promise of lightweight, strong and corrosion resistant Ti alloys with long fatigue lifetimes for automobile or transportation applications has been the vision of the metal industry since titanium came to the attention of scientists and engineers. The sole limitation of realizing these goals has been cost, which is primarily a function of energy used in production. The HSPT process was shown through this work to be capable of realizing this goal, and facilitating the practical use of titanium in US automotive and other industries.

Background

The metal, titanium (Ti) and its alloys, particularly Ti-6Al-4V, are of exceptional value to industry, military and consumer applications. Due to their high cost, which is substantively due to the high embodied energy and production costs of Ti, these alloys do not see the widespread use that their inherent mechanical and physical properties suggest. In particular, applications benefiting from lightweight materials for transportation are the focus of the present study. With successful completion of this project, overall production costs will be substantially lowered, primarily due to the use of lower energy processing steps. More critically, by reducing the weight of automobiles and trucks, the fuel usage for such vehicles will be reduced over the entire lifetime of the vehicles. Additionally, reduced cost for Ti components will likely lead to expansion in the range of viable applications across a number of engineering industries.

The titanium family of alloys has exceptional potential for expanded use in industry. In particular, commercially pure (CP) Ti has a substantial base of current applications in chemical processing industries. Because of its corrosion resistance and biocompatibility, as well as exceptional specific mechanical properties, CP-Ti is commonly used in biomedical and dental applications as well. Due to its excellent corrosion resistance in sea water, CP-Ti sees extensive use in offshore drilling platforms and sea vessels, more so than any other Ti alloy [1]. As the last half of the 20th century brought effective solutions to the technical problems associated with producing and processing titanium alloys, the major remaining obstacle to their widespread use in more moderate environments and stress regimes is cost [2-5].

Powder metallurgy (PM) approaches have been carefully investigated, and in many cases put into production, due to their capacity for fabricating near-net-shape components in a range of alloy systems and ceramics, including: steels, copper, nickel based superalloys, refractory metals, and tungsten carbides. The capacity of PM technologies to produce complex shapes in, or near, their final dimensions can represent substantial cost savings during manufacturing, and in Ti and Ti alloys can eliminate excessive machining and avoid some of the costs associated with ingot metallurgy and wrought processes. In certain aerospace applications, PM technologies could reduce the percentage of scrap during processing from the astounding current rates, as high as 90% or more, down to less than 10% [6]. In this interest, a number of research groups around the world have been pursuing avenues to obtain high density PM Ti processes across the range of Ti alloy compositions.

Hydrogen has played a key role in advancing titanium processing, particularly in new PM technologies where it is beneficial in terms of powder production. While hydrogen in excess of 100-200 ppm can have a negative impact on mechanical properties, especially ductility, this aspect of brittleness has been useful in producing smaller powder sizes by facilitating crushing and grinding of powders while in the form of titanium hydride (TiH_2) [7]. While hydrogen dissolves easily in Ti, it is also readily removed by vacuum. In this regard, early work with hydrogen focused on its use as a temporary alloying element in Ti alloy forgings and castings, where it reduces the flow stress and/or minimum temperature during forging operations [8, 9]. The method is referred to as thermohydrogen processing (THP), and a comprehensive review was compiled by Froes et al. [10]. Additionally, hydrogen was determined to be useful in refining microstructure in Ti-6Al-4V due to the eutectoid transformation, approximately 800 °C, and thus improves mechanical properties [9, 11].

More recently, the role of hydrogen in the form of titanium hydrides has been investigated in PM Ti alloys, allowing increased density from press and sinter methods.[12-15] Greenspan et al. demonstrated TiH2 consolidation through vacuum hot pressing with good strength and ductility [16]. A large body of work was undertaken on hydrides in subsequent decades showing improved sinterability with low porosity levels. In an investigation comparing the density and mechanical properties of several conventional Ti powders to TiH2 powders during PM processing of Ti-6Al-4V, the TiH_2 produced higher densities after vacuum sintering than Ti powders (some samples > 99%), despite having lower densities in the green state [15]. The improved reduction in porosity was hypothesized to be due to hydrogen cleaning of the surfaces during sintering [12, 17, 18], which resulted in improved strength in tensile tests. Wang et al. recently examined densification of different TiH_2 particle sizes through dilatometer and thermogravimetric analyses, and showed that nano-sized particles reached full density more rapidly during sintering, and similar to other researchers found that Ti hydrides resulted in nearly full density for both CP-Ti and Ti-6Al-4V [19].

A new method combining hydrogen sintering, rather than vacuum sintering, with a titanium hydride PM approach, reported improved tensile strength and ductility in PM Ti-6Al-4V [20]. The process has been termed hydrogen sintering and phase transformation (HSPT) and reported fine grain microstructures in sintered samples of near full density for both CP-Ti and Ti-6Al-4V. In this process, green compacts of TiH_2 are sintered under a cover gas of argon and hydrogen, then cooled to below the beta transus temperature to undergo a eutectoid transformation, and vacuum annealed to remove the hydrogen. The addition of hydrogen during sintering, at temperatures within the beta phase where the range of hydrogen solubility in titanium is wide, may aid significantly in improved density and grain refinement and thus, mechanical properties. Early results were very promising, and were the foundation for the proposed project that led to the work reported here.

Results and Discussion

Summary of Tasks and Milestones

Task I

Several powders were considered and evaluated, and a single source was selected. We used Reading Ametek Alloys TiH_2 and master alloy (60 Al-40 V) powders, both -325 mesh throughout the project period. All results below, unless noted otherwise, were obtained using these materials as originating feedstock.

Task II

Samples were tested for density using Archimedes method. Samples were also cut and metallographically polished for grain size measurement. Sections from tensile bars were sent to an independent testing laboratory and/or were tested at the University of Utah for bulk chemical analyses. Sample chemistries tested on site were generally later in the year, after we had acquired the Leco determinator for oxygen, nitrogen and hydrogen. Results of documentation methods are given below.

- *Density:* the average of all samples made since October, 2012 has been 98.9%, and most samples made in 2014 and 2015 have measured at a density of 99.2% or greater.
- *Grain size:* Alpha and beta grains were manually measured separately, given their relative differences in morphology and contrast mechanism using SEM micrographs taken on a Zeiss Quanta high resolution SEM at the University of Utah, and both Ti phases easily met the milestone criteria:
  Alpha grains were measured with an average thickness of 1.2 µm and length of 2.0 µm
  Beta grains were measured with an average thickness of 0.5 µm and length of 1.6 µm
- *Oxygen%:* the average of seven samples produced and tested in 2013 was 0.28%
- *Hydrogen, nitrogen, and carbon content*: Table 1 shows that for averages of samples tested since the project start, all meet or surpass ASTM B348, Grade 5.

Table I – Hydrogen, nitrogen and carbon concentrations of HSPT samples, as well as ASTM B348 specifications.

Element	ASTM B348, Grade 5	Average HSPT Sample
Hydrogen	<0.015	0.0011
Nitrogen	<0.05	0.0214
Carbon	<0.08	0.04

Task III

From the SOPO, the third milestone and Go/No-Go decision was based on the following criteria, which were met within planned deadlines and are described below.

- *Yield strength: 900 MPa*
- *Elongation: 10%*
- *K_{Ic}:40 MPa.$m^{0.5}$*
- *Fatigue endurance limit: 500-600 MPa.*

Tensile tests conducted at the University of Utah demonstrated properties exceeding the milestones for static properties. The average yield strength of ten samples tested in 2014 was 949 MPa (milestone value of at least 900 MPa) and the average ductility in terms of elongation was 13.1% (milestone value of at least 10% elongation). Of the previous twenty five tensile samples tested, no single sample failed to meet the milestone for yield strength and only one sample, which had been inadvertently contaminated during processing, failed to reach 10% elongation. The trends for both yield strength and ductility, as measured by % elongation, look quite strong compared to other PM Ti-6Al-4V materials and overlap the range of values seen for the more expensive and energy intensive wrought Ti materials.

Fracture toughness testing measured K_{Ic} at 47.8 MPa*$m^{0.5}$. Fracture toughness testing conformed to ASTM E399 standards for fracture toughness. Samples were fabricated and sent to an accredited testing facility, and the average value of 47.8 MPa*$m^{0.5}$ surpasses the milestone value of 40 MPa*$m^{0.5}$.

Fatigue testing was ongoing throughout the second and third years of the project, with emphasis on improving the microstructural features that benefit good fatigue properties, particularly the reduction in size of the largest pores in samples and decreasing total percent porosity. A great deal of success was attained in reducing porosity in the system without degrading other properties through raising oxygen levels. Testing of -400 mesh powders with oxygen at 0.24%, showed very promising results for fatigue testing. Ten samples tested at or above 500 MPa survived under fatigue loading for cycles between approximately 1 million and 10 million cycles. Twenty-three of 26 total, as of the second year of the project, of samples tested had fatigue survival cycles equal to or exceeding the wrought lower limit data of Ti-6Al-4V alloy. Thus, the most recent sintered samples have met the Task III fatigue milestone.

The static mechanical properties outlined for Task III surpassed the set Milestones, as discussed below, and Year 2 efforts focused primarily on improving fatigue properties. Fatigue properties are critical for many applications in the auto industry, and are a crucial aspect of component design. Since fatigue properties are generally tied directly to the size and distribution of pores in final components, research efforts in Year 2 involved extensive experimentation to reduce the size and volume percent of pores in these materials while maintaining the low oxygen content, meeting the ASTM specification. Several paths have been pursued in this regard with very promising results, particularly for a new powder processing route that involves milling in a solvent blend media. A fatigue endurance limit of 500 MPa was achieved in 2014 for hydrogen sintered Ti-6Al-4V alloy samples with several specimens enduring (surviving without fracture) for 10^6-10^7 cycles at cyclic stresses in the range of 500 to 600 MPa. This level of fatigue performance indicated that the material had met the Task III milestone, and that the fatigue properties obtained from the HSPT process are competitive with those from the more expensive wrought processing or HIPed PM processes.

In the interest of obtaining the best properties, and range of possible properties, for this process to facilitate commercialization of the HSPT method, fatigue properties and static properties were continually pushed forward throughout the third year. Additionally, post-sintering processes to close remaining porosity though pneumatic isostatic forging and to modify microstructures using heat treatments often used with wrought materials were investigated. Results were very promising for these relatively low energy steps are presented below.

Task IV - Commercialization

With movement of the project into its third year, emphasis was placed on commercialization. In addition to interest from Tier One auto parts suppliers, Reading Alloys entered into discussions and negotiations with the University of Utah's Technology & Venture Commercialization Office and signed an option for licensing of the technology in spring of 2015.. Consideration of markets and products outside the limited licensing agreement signed by Reading Alloys with the University of Utah are ongoing, and the team intends to find other potential licensees over the coming year.

Public releases of the successes in mechanical properties achieved during the project and the reduced production costs of the process have been submitted to DOE and to trade publications, and a slide deck was prepared for DOE for potentially interested industrial contacts. Information on the technology was also made available to the University of Utah's Office of Technology & Venture Commercialization, which leads such efforts in collaboration with the PI for such endeavors.

Task V - Produce prototype components for selected specific applications

Task V.1 - Design a conceptual commercial production line.

Efforts have continued to identify appropriate furnaces and process sequences to develop a viable production train for the HSPT process. In this effort the research group at the University of Utah is interfacing with the project partner, Reading Alloys, in order to mesh expertise within our research group on details of the HSPT process with engineers at Reading Alloys who have access to knowledge and experience related to industrial design and practical application of the technology. Figure 1 shows a schematic of the full process train from powders to sintered parts ready for final machining.

The initial draft process was based on an estimated annual gross of $5 million/year, which after subtracting average corporate tax and profit gives an annual net production of approximately $3 million/year operating on one shift/day. Figure 4 shows a rough schematic view of the necessary steps of production. Analysis assumes a powder cost of $50/kg for raw materials, and would be producing automotive connecting rods with a mass of 347 g and dimensions of approximately 19 x 8 x 3 cm.

Since the project has now moved into an option for licensing phase, efforts to complete the draft commercialization plan were modified to more accurately synchronize with Reading Alloy's engineering team. In that context, some initial assumptions on part geometry and size may change, and we have determined that the upcoming meetings between Reading Alloys and the University of Utah should provide information that will make efforts in this subtask much more useful to initial investors in the technology.

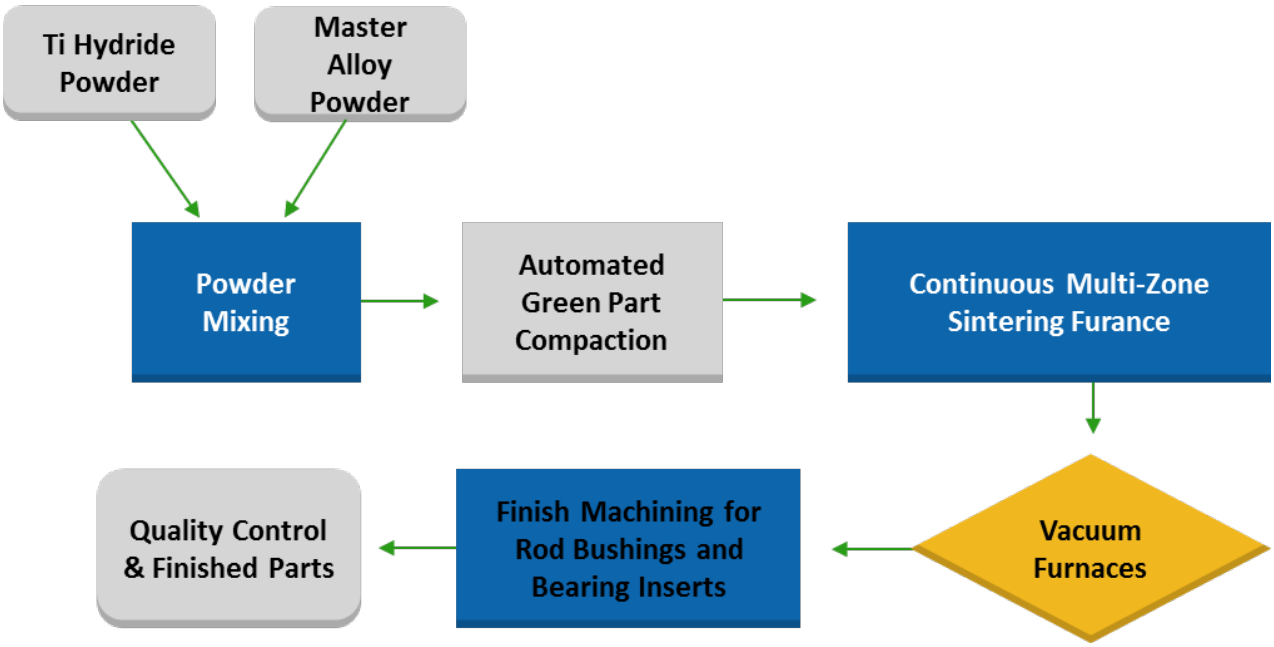

Fig. 1. Schematic of the industrial process train for HSPT.

Results and Discussion of Specific Properties and Processes for HSPT Ti-6Al-4V

Powder Processing

It is noteworthy that titanium's high cost is principally due to its high affinity for interstitial elements, such as oxygen [21]. With increasing oxygen content in titanium alloys, the yield strength and hardness increase, but with a corresponding decrease in ductility [22]. Generally, oxygen levels in sintered titanium parts depend on the powder production method, particle size of powders, compaction, as well as sintering parameters and other process considerations. As the powder particle size becomes finer and the specific surface area increases, there is an increase in oxygen content since oxygen is entrapped in a passivated film near the surface of titanium powders. Larger particles show lower oxygen content after sintering, but the sinterability and porosity of sintered parts become a major issue; while finer particle sizes are more desirable to reduce porosity and attain full density. Thus, oxygen levels must be maintained within lower ranges to achieve desired mechanical properties for most applications.

A number of techniques for reducing oxygen content in powder metallurgy (PM) Ti have been studied in recent years [23-25]. The effect of introducing rare earth elements including Nd and Y to deplete oxygen in titanium alloys has been examined [23, 25], and the cleaning effect of hydrogen on oxygen content during sintering titanium hydride was also investigated [24]. Aside from using additives as oxygen getters, several researchers have reported on the contribution of different powder metallurgy processing steps to the level of oxygen [26-28].

Since oxygen plays such a pivotal role in mechanical properties of Ti alloys, our group investigated alternate milling environments for the milling of Ti and master alloy powders in the

present project. Particularly of interest were materials that would impede oxygen diffusivity, with promising results obtained from light mineral oil (LMO) and heavy mineral oil (HMO). Figure 2 shows baseline results from these experiments, indicating that powders could be milled to finer size, which encourages lower porosity in the final sintered samples, without raising the oxygen level as much as other milling environments.

Having discerned the potential of LMO to act as a superior environment for milling of powders, reducing the size of powders effectively while maintaining lower oxygen contents than other milling environments, we conducted further experiments on conventional methods vs. milling in LMO. Figure 3 shows results of attritor milling experiments using heptane (the standard environment for many applications), dry milling and light mineral oil. Particularly for finer particle sizes, which yield lower porosity in final sintered parts, Fig. 3 shows significantly lower oxygen for a given specific surface area compared to either milling in heptane or for dry milling.

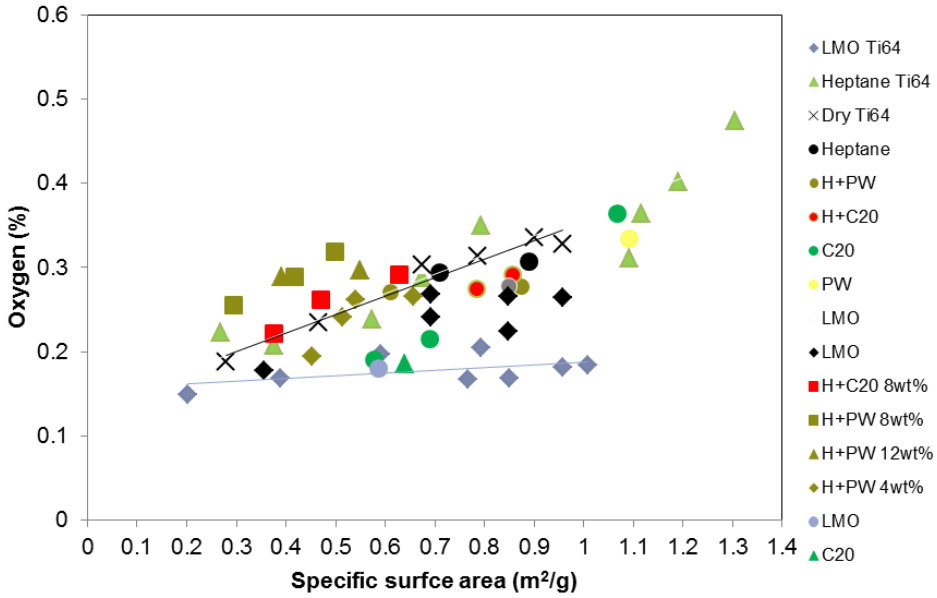

Fig. 2 Relationship between specific surface area and oxygen contents of the attritor milled Ti-6Al-4V for powders milled in heptane, LMO, wax and dry milled in Ar.

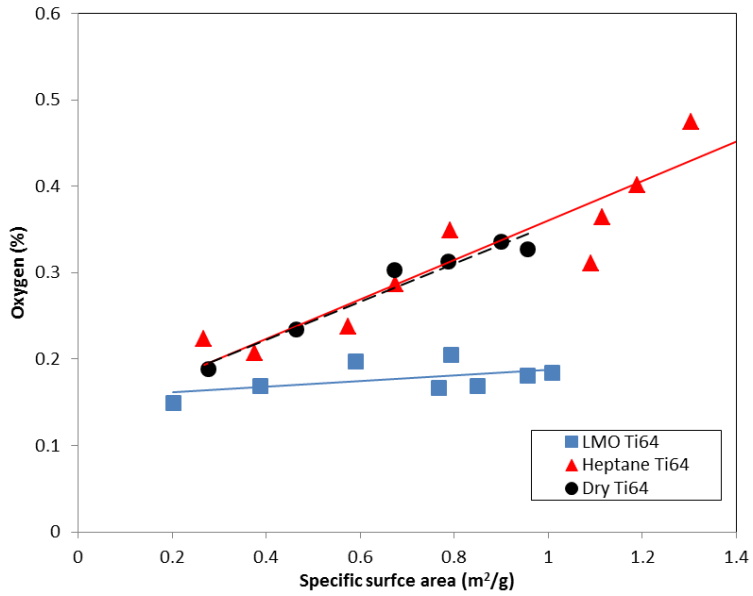

Fig. 3. Relationship between specific surface area and oxygen contents of the attritor milled Ti-6Al-4V for powders milled in LMO, heptane and dry milled in Ar.

Phase Equilibria and Transformations

The primary advancement of the HSPT process over competing PM technologies is its capacity to produce fine grained microstructures in the as-sintered state. This is directly the result of phase transformations that occur during processing due to the addition of a hydrogen atmosphere. Examination of the phase diagrams for the (Ti-6Al-4V)-H system available in the literature showed great disparity and several studies appeared to utilize less than optimum experimental procedures. Given the industrial relevance of this materials system, it was desirable to develop a more accurate near equilibrium (Ti-6Al-4V)-xH phase diagram, using a direct approach to determine equilibrium phases at elevated temperatures in hydrogen atmosphere with controlled partial pressures of H_2.

In this work, a high energy synchrotron X-ray source was used to determine equilibrium phases in titanium materials *in situ* at high temperatures and at various hydrogen pressures. Compared with conventional laboratory XRD techniques, high energy synchrotron radiation has a larger penetration depth and better spectral resolution in metallic materials, and allows direct observation of equilibrium phases in bulk Ti-6Al-4V during hydrogenation or dehydrogenation. Further, its high acquisition rate provides a clear observation of the sequence of phase transformations in real time under changing conditions of temperature or partial pressure of hydrogen. The objective of this work was to determine critical phase boundaries affecting the microstructure of the (Ti-6Al-4V)-xH alloy during cooling from temperatures above 1000 ºC. In order to determine the exact hydrogen content that corresponds to phase change temperatures, thermal gravimetric analysis (TGA) and differential scanning calorimetry (DSC) were also employed.

Figure 4 shows an example of an experiment in the synchrotron X-ray source where a sample was held in a 35% hydrogen atmosphere isothermally at 550° C. The direct observation of phase transformation in real time eliminated the ambiguities encountered by other techniques attempting to discern the phase transformations in this system. Figure 5 shows examples of

different microstructures developed under 100% hydrogen at different temperatures with relevant phases identified. In addition to the phase relationship data points added to the phase diagram by the synchrotron experiments, TGA analysis was also employed to gain understanding of lower temperature transformations. A more comprehensive examination of this portion of the project has been published, and can be found now in the scientific literature [29].

Figure 6 shows the partial phase diagram assembled from the *in situ* high energy X-ray analysis combined with the TGA data. This work significantly enhanced both the basic scientific knowledge and also the practical application of hydrogen technologies in the Ti-6Al-4V system, and assisted in elucidating the phase transformations in this system. Conclusions drawn from the work included [29]:

- The eutectoid phase transformation β ↔ α+δ was determined to be in the hydrogen range of 17.3-45.3 at.%, and the eutectoid point is 37.5 at.% at 211 ºC. A four phase region of α+β+ α2+δ is present below this point in the phase diagram.
- A two-phase β+α2 region is present above the eutectoid point.
- The α2 phase was observed to form at compositions greater than approximately 22 at.% hydrogen, but was not evident after dehydrogenation at 750 ºC.
- The δ hyride phase can be produced in (Ti-6Al-4V)-xH either as a eutectoid transformed product or as primary δ phase transformed from the β pahse.
- The β transus temperature was determined to be between 800 ºC and 850 ºC in the hydrogen concentration range of 9.0-19.4 at.%.

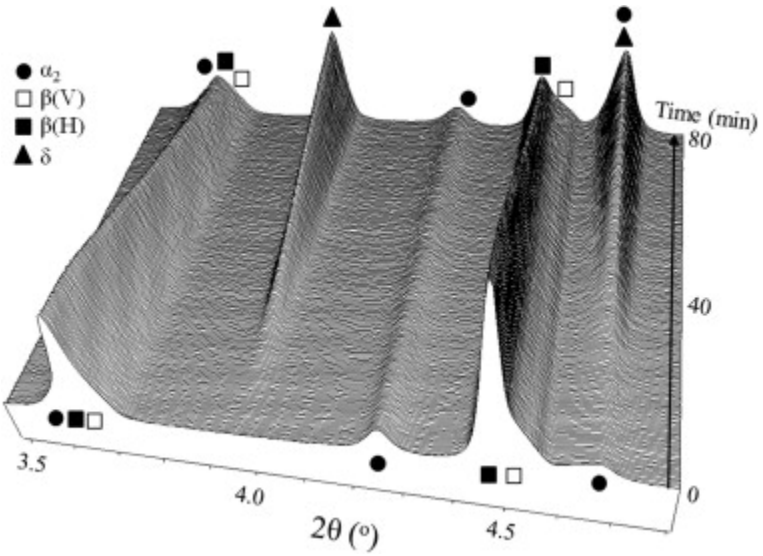

Fig. 4. In situ synchrotron X-ray spectra of formation of titanium hydride during isothermal hydrogenation at 550 ºC in 35% hydrogen.

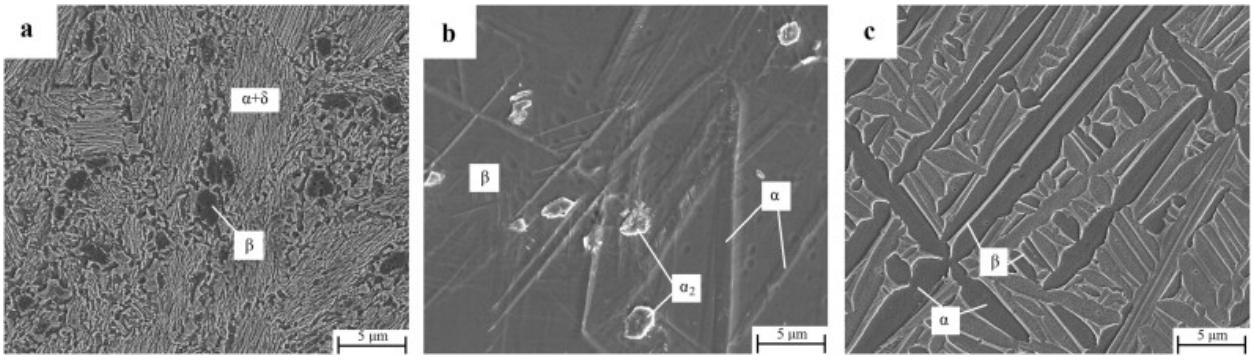

Fig. 5. Microstructures after being hydrogenated in 100% H_2 at various temperatures: (a) 650 ºC, (c) 750 ºC and (d) 850 ºC and cooled in Ar.

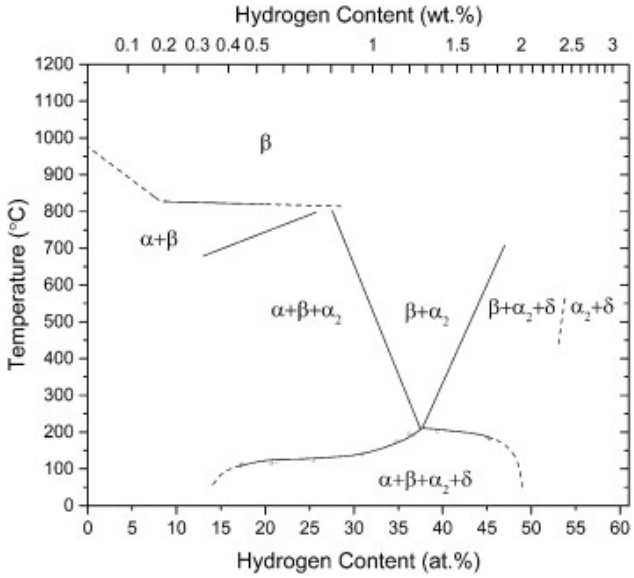

Fig. 6. Proposed partial pseudo-binary (Ti-6Al-4V)-xH phase diagram. Dashed lines delineate phase boundaries that are approximate, and not verified by experimental data.

Microstructural Development

As mentioned earlier, one of the primary reasons for the superior mechanical properties of HSPT produced materials over other lower cost PM processes, particularly vacuum sintering, is the finer grain size. Figure 7 shows examples of the microstructures of these two production techniques. Note the different scale bars, Fig. 7, showing a profoundly finer grain structure in the HSPT sample.

Following work on developing a functional and accurate phase diagram, the group investigated aspects of the microstructural development that were deemed integral to the formation of desired microstructural features, particularly the refined grain sizes of phases present in the final HSPT microstructures. This work has also been published in the literature, and is described there in greater detail. [30]. Figure 8 shows the thermal processing of both

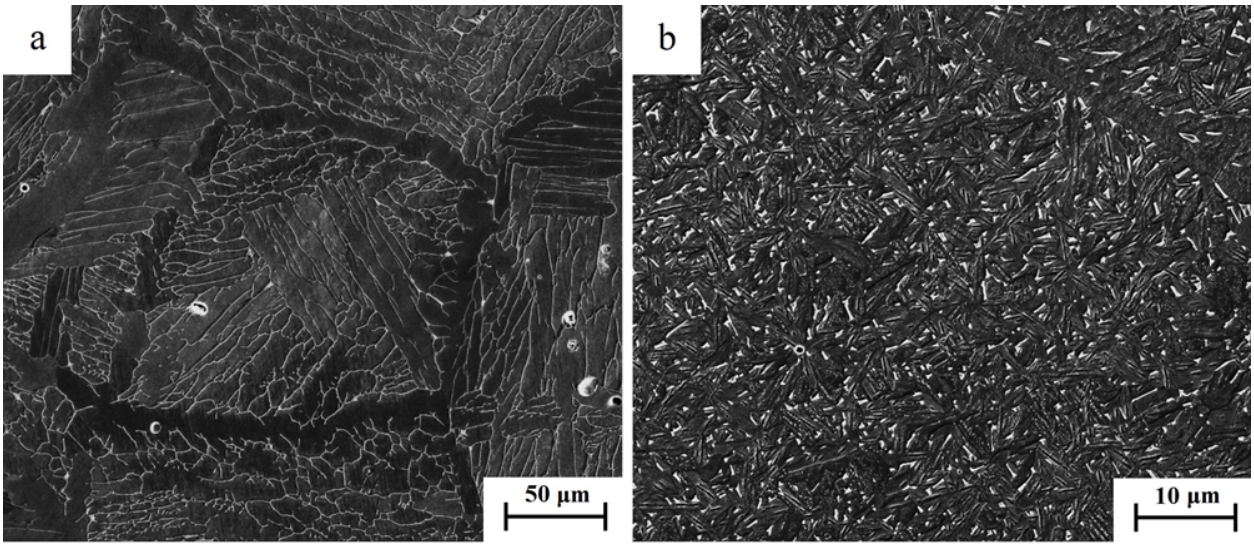

Fig. 7 SEM micrographs of Ti-6Al-4V microstructure by (a) vacuum sintering and (b) HSPT.

vacuum sintered and HSPT produced samples for this work, with the time and temperature of sintering the same for both methods. In HSPT, a subsequent isothermal hold at 650 °C was made for phase transformations to occur, as well as a post sintering dehydrogenation step to remove hydrogen from the samples in order to avoid brittleness in the final material.

Through detailed analysis of the phase transformations and examination of microstructures at various stages, a more thorough understanding of how HSPT develops desired microstructures was obtained. Figure 9 shows an example of TEM work done to determine the nature of submicrometer phases in this system [30]. Electron diffraction pattern indexing was used for identification of various phases.

Figure 10 shows examples of microstructures obtained after dehydrogenation, and after having been isothermally held at different temperatures between sintering and dehydrogenation. These experiments aided in determining the optimum heat-treating to obtain desirable microstructures for best practice HSPT processing.

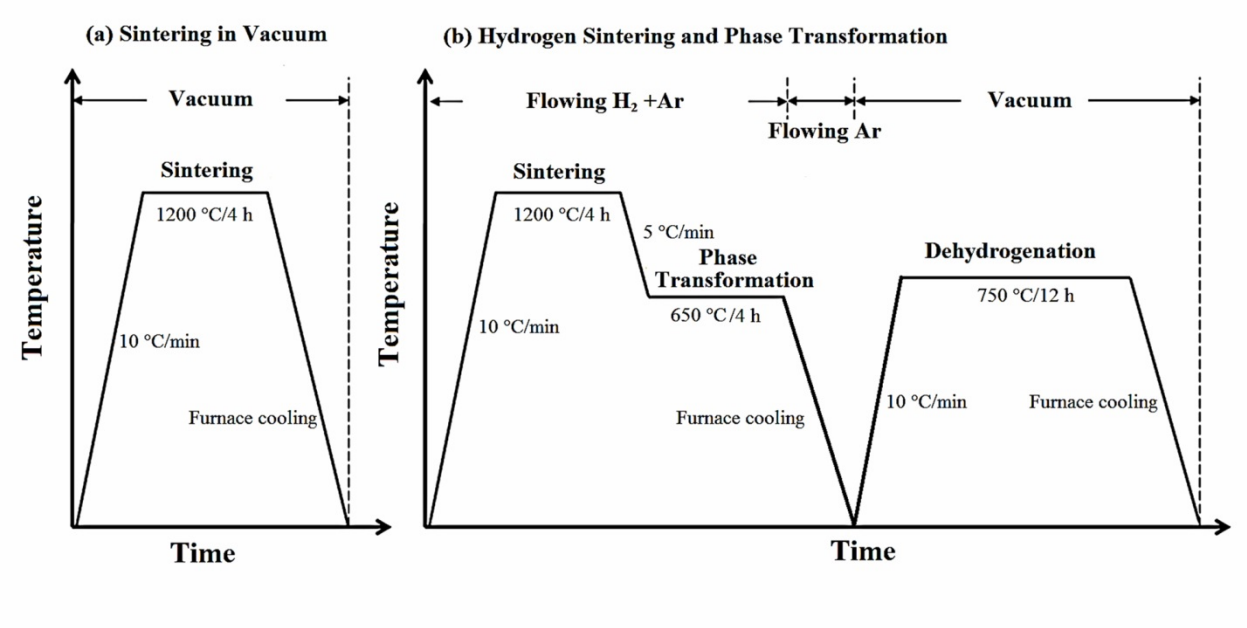

Fig. 8. The temperature-time profiles of (a) vacuum sintering and (b) HSPT.

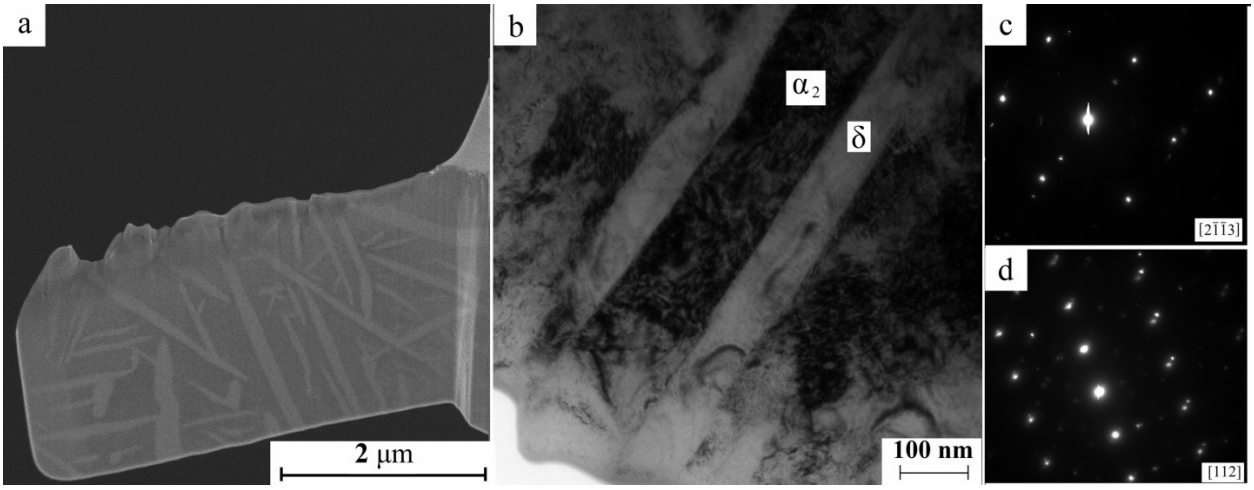

Fig. 9 (a) SEM micrograph of TEM specimen prepared by FIB. TEM pictures of Ti-6Al-4V-H held at 650 ºC for 4 hours before dehydrogenation: (b) bright field, corresponding SAED pattern of (c) the α2 phase, and (d) the δ phase.

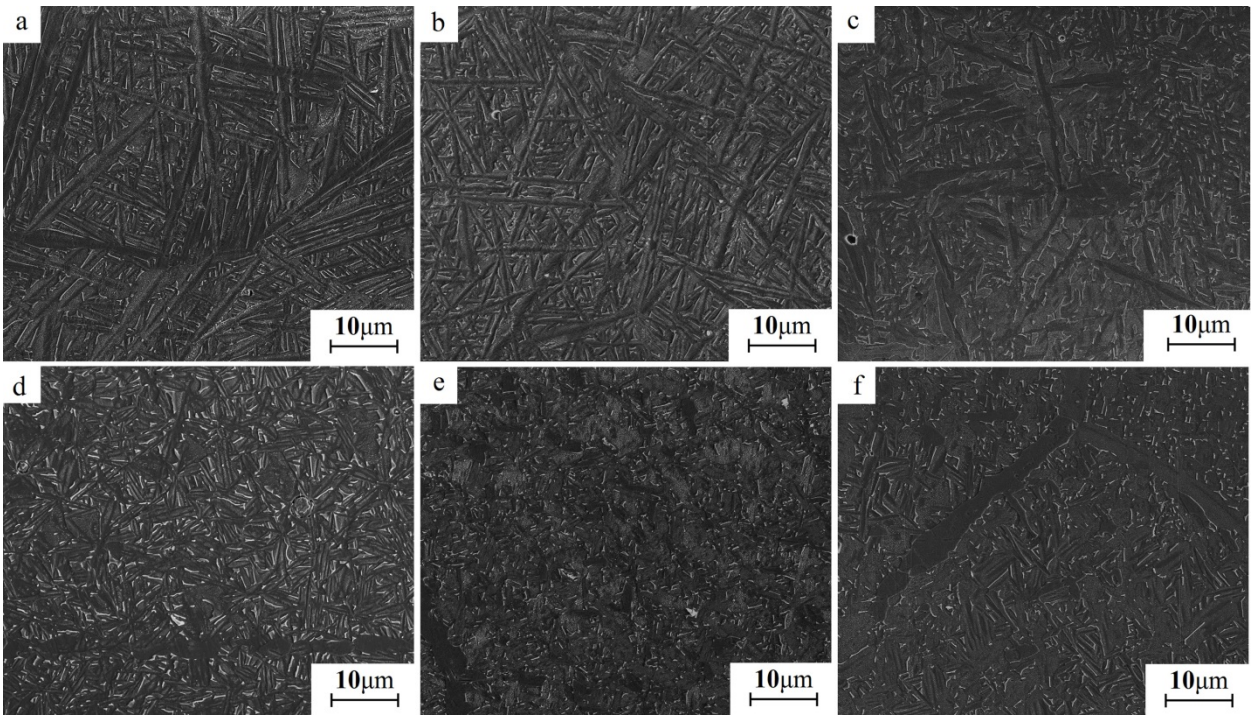

Fig. 10. SEM microstructure of Ti-6Al-4V after holding at (a) 850 °C, (b) 800 ºC, (c) 750 ºC, (d) 700 ºC, (e) 600 ºC and (f) 550 ºC for 4 hours in 50% H2, furnace-cooling to room temperature in flowing argon, and dehydrogenating in vacuum at 750 °C/12 hours.

Primary conclusions from the microstructural development investigations included [30]:

- Ultra-fine microstructures of Ti-6Al-4V can be produced by applying the hydrogen sintering and phase transformation (HSPT) process. The critical factor for forming the ultra-fine microstructure is the isothermal hold temperature which is in the range of 600-700 ºC in 0.5 atm of H2.
- The mechanisms of the microstructural refinement during HSPT are the combined effects of the precipitation of fine α/α2 particles within the β grains, which refine the coarse β grains during isothermal holding, and the eutectoid transformation of remaining β into very fine (α+ δ) at a lower temperature.
- During HSPT, the presence of hydrogen converts the Ti-6Al-4V (a typical α+β alloy) into to a metastable β Ti alloy, hence causing the precipitation of fine α/α2 within β grains.
- The α2 phase is a temporary intermediate phase during HSPT. It forms during isothermal holds under partial hydrogen atmosphere in the temperature range of 750-550 ºC. The α2 transforms to α during dehydrogenation at 750 ºC.

Alternate Microstructures from Post-Sintering Heat Treatments

In order to expand the range of potential applications for HSPT materials, and thereby encourage interest in commercialization of the process, the feasibility of producing a range of wrought-like microstructures via simple heat treatments of as-sintered HSPT Ti-6Al-4V was investigated. The goal of this research was to produce wrought-like mechanical properties

without resorting to energy-intensive thermomechanical work that is compulsory for producing high performance titanium alloys via wrought processing or traditional powder metallurgy. The heat treatments employed are illustrated in Fig. 11, and again, these results have been published in the scientific literature with considerably more detail [31]. In this portion of the investigation, samples were sintered using the same starting powders by both vacuum sintering and HSPT, and then subjected to relatively simple post sintering heat treatments, as shown in Fig. 11.

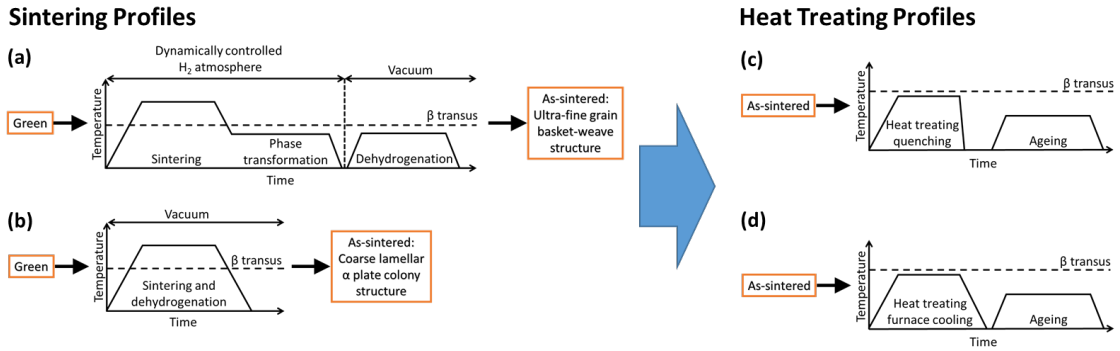

Figure 11: Thermal profiles used for: a) HSPT sintering and dehydrogenation, b) vacuum sintering, c) heat treating with rapid cooling (water quenching), and d) heat treating with furnace cooling.

After heat treating samples, then metallographic preparation, microstructures were examined by both optical microscopy and SEM. Optical micrographs are presented in Fig. 12.

Figure 12-b shows the microstructure of an HSPT-sintered sample after heat treatment with water quenching. Similar to wrought processing, this heat treatment produced a clearly bi-modal (duplex) microstructure. This microstructure consists of globularized primary grains constituting about 40 vol% of the microstructure. The remainder of the microstructure consists of acicular α grains with dispersed retained β. It should be noted that while some of the primary α grains in the heat treated HSPT sample are truly equiaxed (aspect ratio equal to unity), some of the grains are still slightly elongated. It is believed that the morphology of the primary α grains may be further evolved by increasing the high-temperature dwell time during the heat treatment, although experiments have not yet been run to confirm this. The size of the globularized primary α grains is on the order of 2~5 μm, while the acicular α grains have submicron dimensions.

Figure 12-c shows the microstructure of an HSPT-sintered sample after heat treatment with slow cooling. This microstructure resembles a fully-equiaxed wrought microstructure produced via hot working and a similar heat treatment and ageing. Again, while the primary α grains are clearly globularized and have a low aspect ratio, some of the grains are still slightly elongated. Therefore, for this result, it may be said that the microstructure is "globularized", as the definition for "equiaxed" does not strictly apply to every α grain. However, as mentioned above, the morphology of the primary α grains is dependent on the high-temperature dwell time. Therefore, it is believed that increasing this dwell time may produce a microstructure in which all of the primary α grains have a truly equiaxed morphology. After heat treatment, the globularized α grains had an average grain size on the order of 5 μm. The vacuum sintered samples showed much coarser grain size than HSPT, Fig. 12-d, and in the heat treated samples failed to produce the desired microstructural morphologies described above for HSPT samples, Fig 12-e and 12-f, showing very elongated high aspect ratio morphologies.

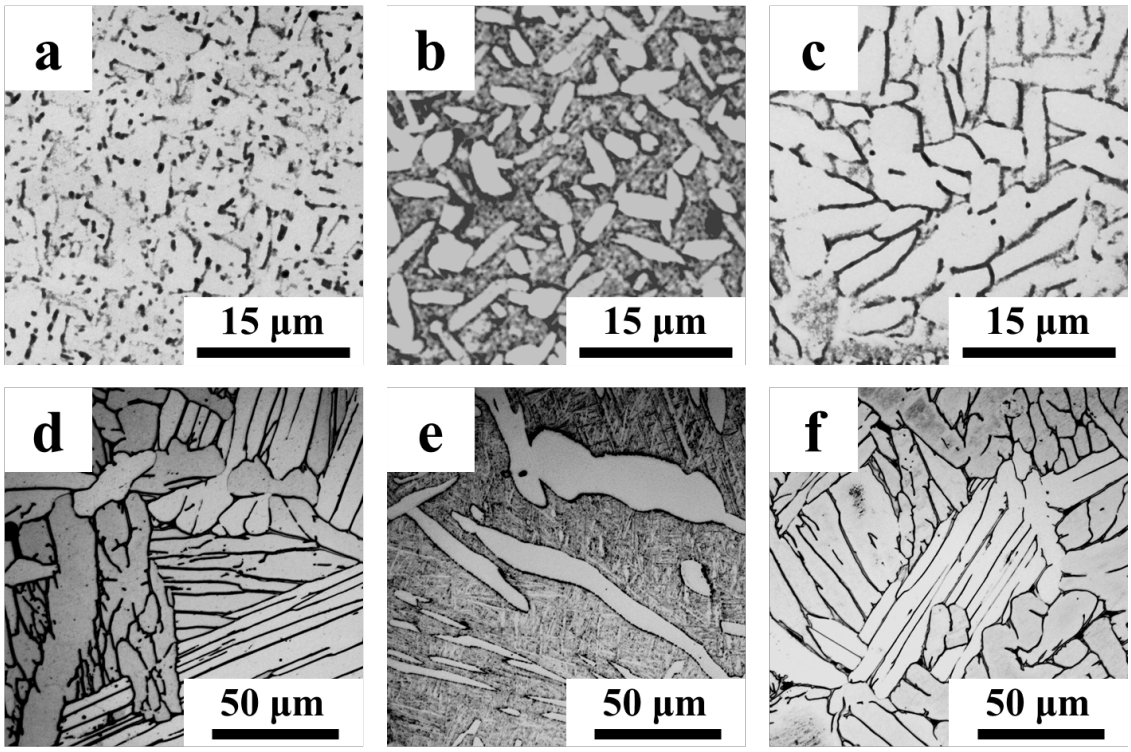

Fig. 12. Optical micrographs of Ti-6Al-4V: a) as-sintered HSPT, b) HSPT after heat treatment with water quench, c) HSPT after heat treatment with furnace cooling, d) as-vacuum-sintered, e) vacuum-sintered after heat treatment with water quench, and f) vacuum-sintered after heat treatment with furnace cooling.

Tensile Properties

Although the preponderance of work performed in the project centered around the most widely used alloy system for titanium, Ti-6Al-4V, significant work was also done on commercially pure Ti (CP-Ti), which also sees significant industrial application. The HSPT process applies equally well to CP-Ti, resulting in very fine grain microstructures, as with the Ti-6Al-4V. Table II shows minor element concentrations, tensile strength, yield strength and ductility (both elongation and reduction in area) for both vacuum sintered and HSPT samples. These values are compared to Grade 2 and Grade 3 CP-Ti. As can be seen in Table II, the HSPT samples surpassed both grade standards and the vacuum sintered samples for both strength and ductility.

In terms of tensile properties from Ti-6Al-4V, samples have been prepared and tested from as-sintered HSPT processing, as well as with the additional heat treatments described in the previous section on alternate microstructures produced by post-sintering heat treatments. Figure 13 shows static tensile property measurements of as-sintered HSPT samples of Ti-6Al-4V compared to wrought samples for yield strength vs. ductility measured by percent elongation. The HSPT samples show exceptional strength with acceptable ductility, overlapping the upper range for strength in the wrought material. There is an inverse relationship between ductility and strength in these materials, and increased oxygen content raises strength, while lowering ductility. These HSPT samples had slightly elevated oxygen, but the fact that the HSPT data

meshes with the much more expensive wrought processing is very encouraging for the lower cost HSPT process.

Table II. Impurity concentrations and tensile properties of vacuum-sintered and hydrogen-sintered CP-Ti.

	Tensile strength (MPa)	0.2% Yield strength (MPa)	El (%)	RA(%)	O (wt%)	H (wt%)	C (wt%)	N (wt%)
Grade 2	345	275	20	30	0.25	0.015	0.08	0.03
Grade 3	450	380	18	30	0.35	0.015	0.08	0.05
Vacuum sintered	602±14	459±17	20±4	26±3	0.283 ±0.023	0.0003 ±0.0001	0.066 ±0.010	0.027 ±0.011
HSPT*	687±13	568±5	24±4	35±12	0.280 ±0.08	0.0018 ±0.0010	0.063 ±0.003	0.034 ±0.003

* Dehydrogenation condition: 750°C/12 hours at 10^{-3} Pa; four tensile bars were tested to get the average tensile properties.

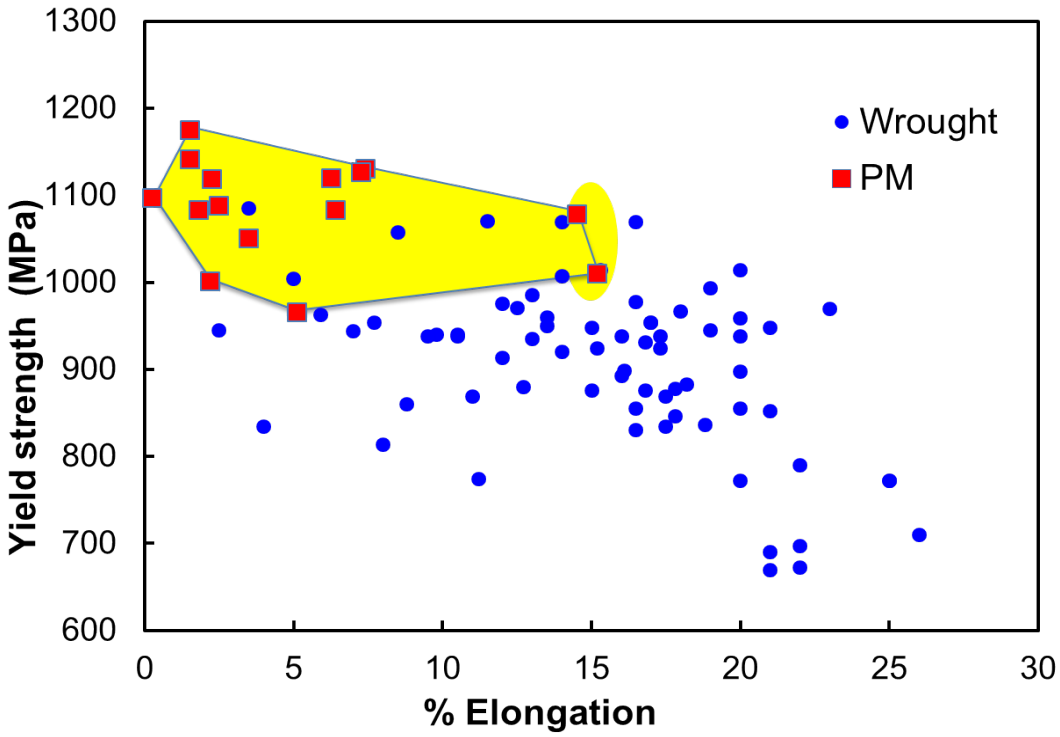

Fig. 13. Tensile data on strength and ductility of HSPT Ti-6Al-4V samples (range shaded in yellow), compared to wrought samples.

Figure 14 shows example tensile test curves from representative samples of as-sintered HSPT samples, as well as stress-strain curves for the two post-sintering heat treatments described in the previous section on alternate microstructures. Differences in strength and ductility between the 3hree conditions can be readily observed. These variations in readily obtained properties, summarized in Table III, give a broader range of desired mechanical properties that can be tailored to particular applications. It should be noted that strength values for HSPT samples are significantly higher than the ASTM standard, and surpass the strength of wrought samples, while maintaining comparable ductility. These are genuinely exceptional results for any PM Ti material, and even more profound considering the lower cost production methodology.

Table III. Range of tensile properties for Ti-6Al-4V produced via HSPT, typical values from literature for wrought Ti-6Al-4V after various heat treatments, and the ASTM standard for annealed grade 5 Ti-6Al-4V. Note: the HSPT tensile data shown here is from sub-size ASTM E8 tensile bars with a 6.35 mm diameter by 25.4 mm long gauge.

Condition	UTS (MPa)	$r_{y,0.2\%}$ (MPa)	Elongation (%)
HSPT			
As-sintered HSPT	994–1024	930–974	13.8–17.8
Bi-modal	1070–1076	981–981	10.7–11.9
‘‘Globularized’’	949–952	872–881	17.6–19.2
Wrought			
forged + recrystallization annealed	876	711	12
forged + solution treatment and age	938	876	15
forged + duplex annealing	911	856	15
ASTM standard B348 (Grade 5 Ti-6Al-4V)	895	828	

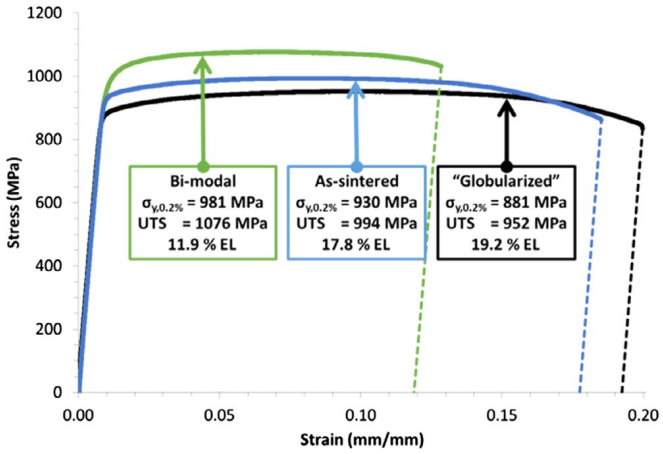

Fig. 14. Representative engineering stress–strain curves of HSPT Ti-6Al-4V with the as-sintered, ‘‘globularized’’, and bi-modal microstructures shown in Fig. 12 a–c, respectively.

Tensile Properties and Pore Size

As mentioned earlier, porosity is often a limiting factor in the application of powder metallurgy components in mechanical applications. In addition to crack initiation, it was

observed that there was a potential link to limitations of ductility in these materials. Therefore work was undertaken to investigate the effects of porosity in general, and particularly of the largest pores found on the fracture surfaces of tensile test samples. These largest pores were termed “extreme sized pores,” and a journal article has been written and sbumitted. This journal article is currently being reviewed for publication at the time of this report’s drafting.

Figure 15 shows examples of polished cross sections of tensile bars and shows the general microstructure, including grain boundary alpha, as well as typical porosity in these samples of Ti-6Al-4V with slightly elevated oxygen. The pore distribution in this image is given in Fig. 15 (a), including arrows for the individual larger pores. Although there were not many pores in excess of 20 μm in this particular sample, it was hypothesized that these largest pores might have an effect on ductility.

Figure 16 shows the variation of several mechanical properties to the extreme-sized pores in those samples, as well as the true stress-true strain curves for all samples in this portion of the study (Fig. 16 (a)). Note the wide variation in ductility, measured by strain to failure in these samples, produced from the same powders and under the same processing parameters. When examining the pores from the fracture surfaces of these tensile samples, it was noted that there were marked differences in pore morphology and aspect ratio. Samples were divided into three groups, illustrated in Fig. 16 (d), on this basis. It is of particular note that strength did not correlate to these large pores, but rather only the ductility of the samples as measured by strain. Although these samples were all produced from titanium hydride powder with slightly elevated oxygen, which in itself decreases ductility, the following conclusions were drawn regarding materials of this composition:

- Extreme-sized pores lead to a rapid decrease in tensile ductility of the PM Ti-6Al-4V alloy. Three distinct trends of decreasing ductility with increases in the extreme pore size were seen and were classified on the basis of the type of extreme-sized pores found in the material.
- Neither the volume fraction of pore nor the extreme-sized nature of the pore affects the tensile strength properties in the material. The strength properties remained nearly constant in all specimens.
- Fracture always initiated from an extreme-sized pore in the material with the remaining smaller pores did not play a significant role in affecting the tensile properties.

It should also be noted that per the preceding section on tensile properties of HSPT samples in general, consistantly much higher ductilities were observed from samples with oxygen within ASTM B348 compositional specifications.

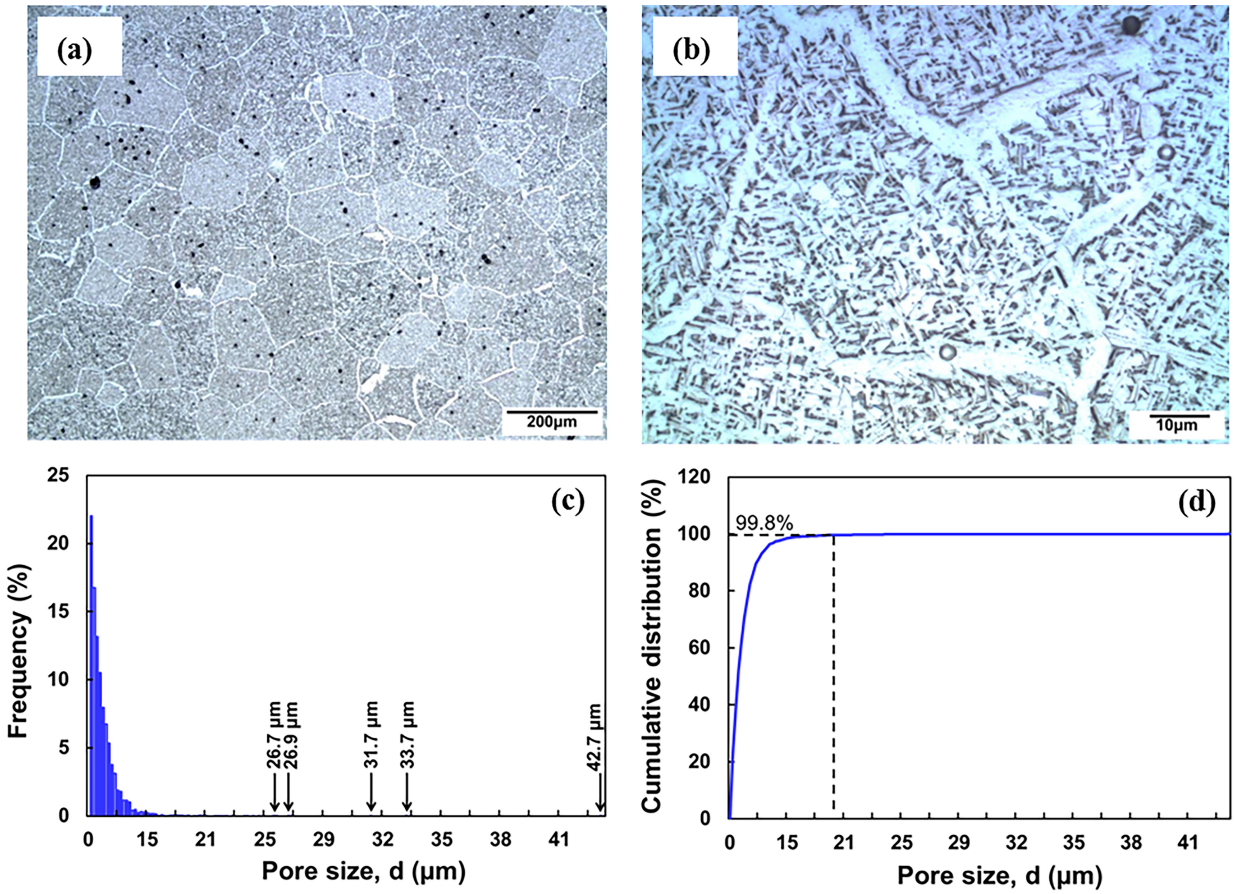

Fig. 15. (a) Optical microstructure showing prior beta grains, (b) sturcture of matrix and grain boundary-α, (c) frequencey of occurrence of pores by size, and (d) cumulative pore distribution of HSPT process Ti-6Al-4V. Note: the arrows in (c) indicate the sizes of a few individual extreme-sized pores.

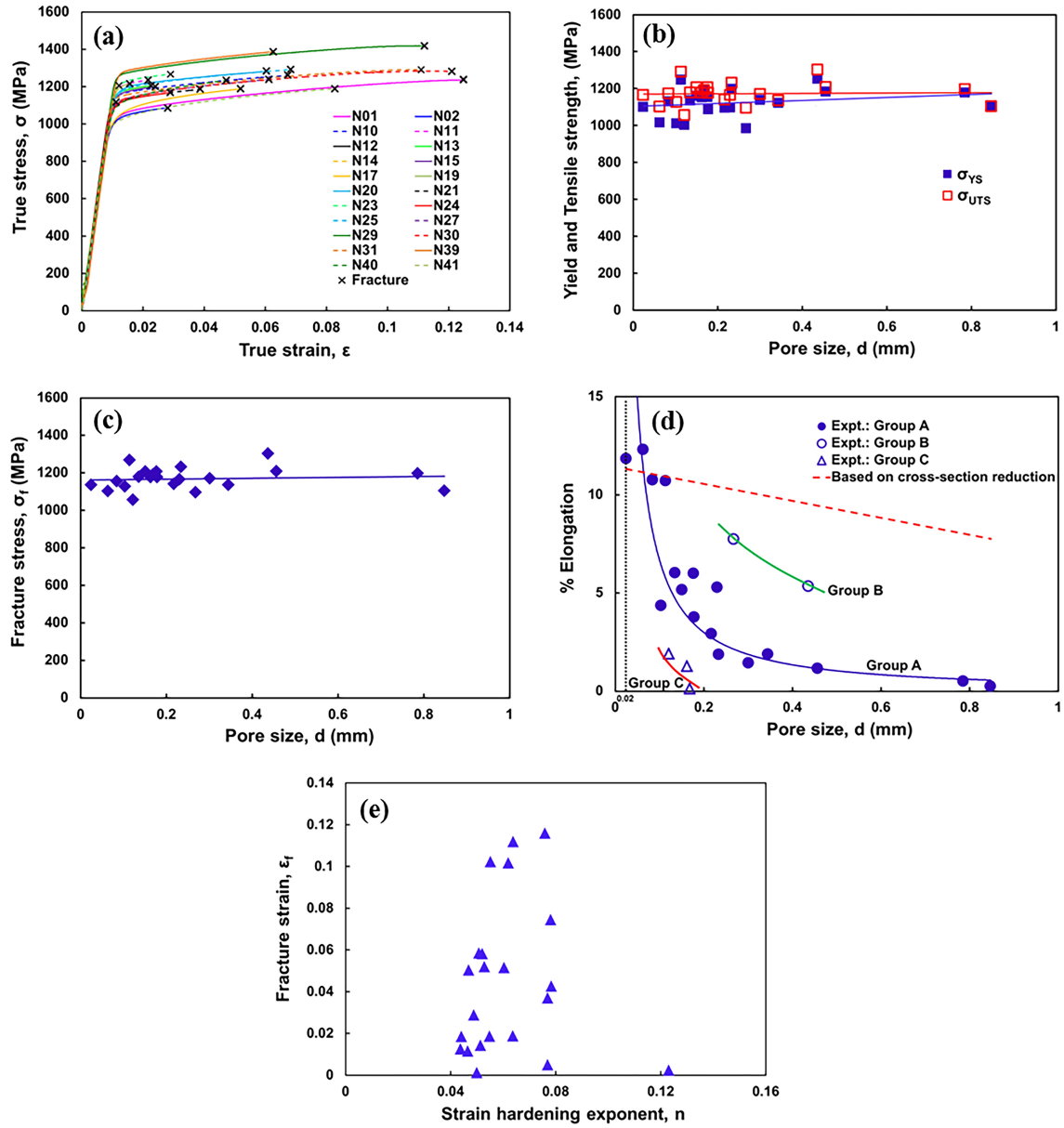

Fig. 16. (a) True stress-true strain thesile curves; (b) through (d) show the variations of yield strength, ultimate tensile strength and fracture stress as well as percent elongation as a function of the size of the largest pore from which failure occurred; (e) demonstrates the lack of a correlation between fracture strain and strain hardening.

Fatigue Properties

Although not crucial for many applications, good fatigue performance is important for most load train applications and for other parts seeing cyclic stress regimes. As mentioned earlier, PM materials are not well known for excellent fatigue performance, primarily due to residual porosity in the final microstructure, but also from other microstructural features such as grain boundary alpha phase. As with the previous section on tensile properties of slightly elevated oxygen samples, the largest pores in fatigue samples generally act as nucleation sites for the initiation of cracks that grow until they eventually cause failure. Thus, a main microstructural emphasis of this project was to reduce porosity and maximum pore size, while simulatneously

measuring the fatigue properties and elucidating the relationships involved between microstructure and fatigue performance.

In PM materials, principally two approaches, namely, the blended elemental (BE) powder approach and the pre-alloyed (PA) powder approach have been undertaken to make PM titanium components. In the BE approach, titanium and component powders, required to make an alloy of specific composition, are blended, compacted and sintered at a sufficiently high temperature (usually in the beta-phase field) to get the final alloy. In the PA approach, the powders of the required alloy composition are first made by atomization of the liquid alloy, followed by consolidation of powders by sintering. The PA products typically have superior mechanical properties than BE products due to a finer grain size (primarily due to faster cooling rates in the atomization of powders) and uniformity of composition resulting from the fully melted alloy. However the costs of PA products are significantly higher, for reasons that are obvious from the steps of the method. Therefore, BE method has been the generally-preferred method to make PM titanium alloy parts [31]. However, the main drawback of the conventional BE PM method is that, due to the necessity to sinter in beta-phase field (>1373 K (1100 ˚C)), it leads to a coarse colony microstructure with aligned α-platelets and a thick layer of grain boundary α phase [32-34]. Both of these microstructural features are detrimental to high cycle fatigue strength--it has not been possible to achieve fatigue limits (at 10^7 cycle endurance) in excess of 400 MPa. Since titanium alloy parts, especially in aerospace and potentially in automotive, are used in fatigue critical components, PM process innovations, targeted to refine the microstructure of PM titanium alloys, are necessary to improve the HCF strength to effectively compete with wrought titanium alloys.

Samples were prepared from powders with different size distributions in an attempt to affect the porosity level, and potentially therefore the fatigue properties. Finer powders compact more readily, generally resulting in lower porosity in the final sintered parts. Figure 17 shows microstructures of 400 mesh (finer powders), 325 mesh (slightly coarser powders) and a sample from 400 mesh powder that has had most of the residual porosity closed by pneumatic isostatic forging (PIF).

The samples made with 400 mesh powder did show slightly lower overall porosity and smaller maximum pore size, and also showed better fatigue performance with an endurance limit approximately 75 MPa higher than that obtained from samples made from 325 mesh powder. The samples that had been PIFed showed significantly better fatigue performance than either of the other two sample sets, particularly under stresses between 650-800 MPa, where they survived 1.5-2 orders of magnitude further cycles to failure than samples that had not had a PIF treatment. Under further cycling, however, curves for all three samples appear to converge above $1.0*e^6$ cycles. It is hypothesized that eventhough most of the porosity has been closed in these samples by PIF, there may not be sufficient time and temperature in the process to allow full diffusion bonding of the pore walls to one another.

Figure 19 shows s-n curves for the two HSPT sample sets without PIF, compared to mill annealed wrought material, which still shows superior fatigue performance, particularly at higher cycles. However, Fig. 19 also shows HSPT's superior performance to all other PM processes that have been documented in the literature.

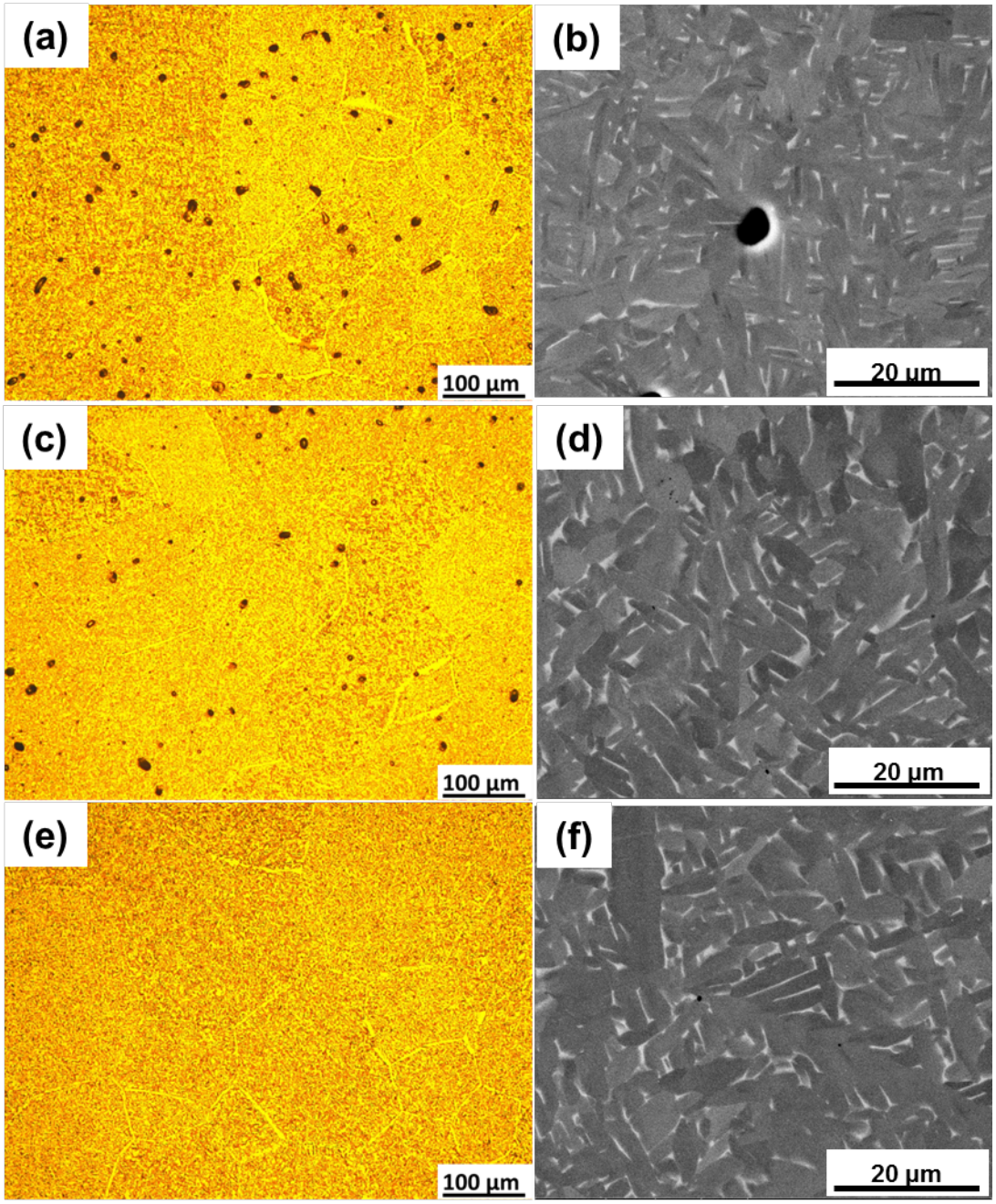

Fig. 17. Optical and SEM micrographs of Ti-6Al-4V alloys after sintering and dehydrogenation and made with, (a,b) -325 mesh powder (4 hr), (c,d) -400 mesh powder (8hr), and (e,f) -400 mesh powder (4 hr) followed by PIF consolidation.

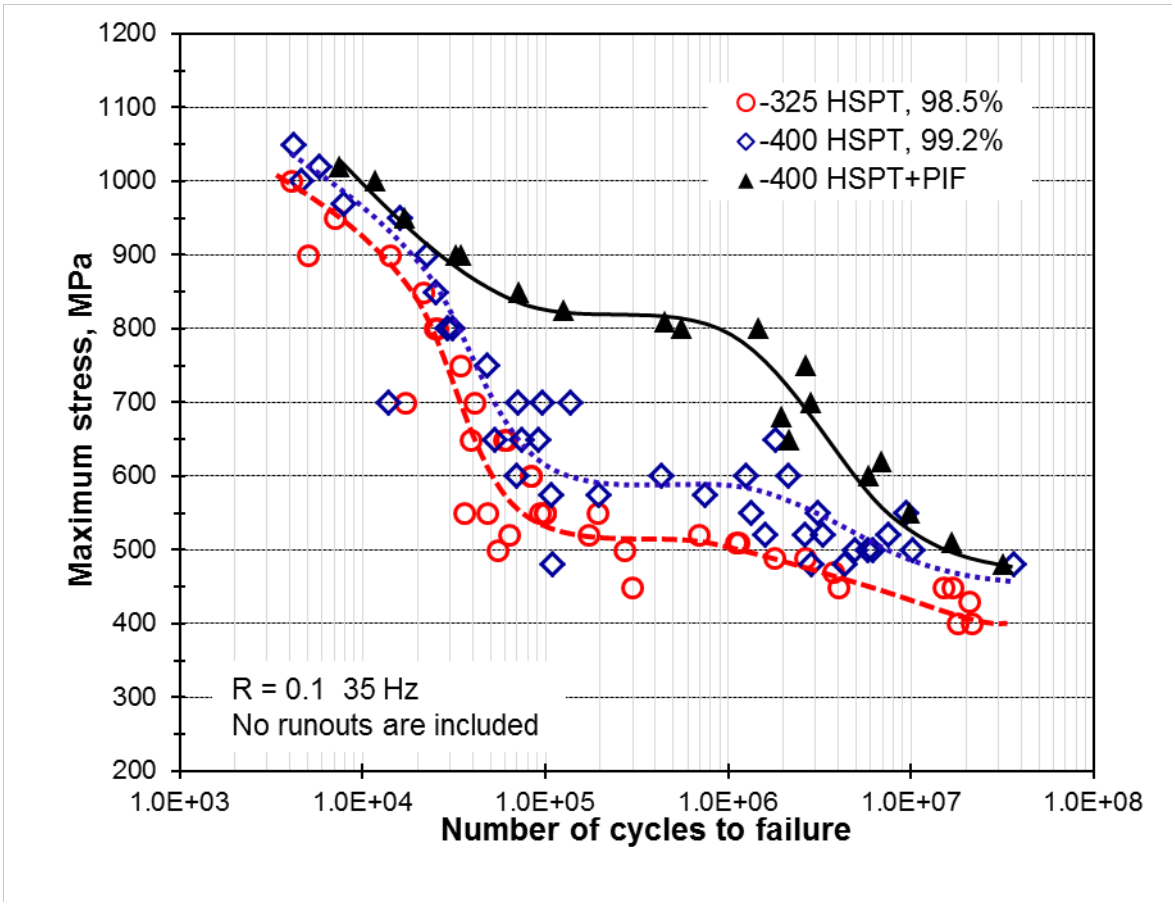

Fig. 18. The S-N curves for the PM Ti-6Al-4V alloy made using 325 mesh powder, 400 mesh powder and 400 mesh powder followed by a PIF step.

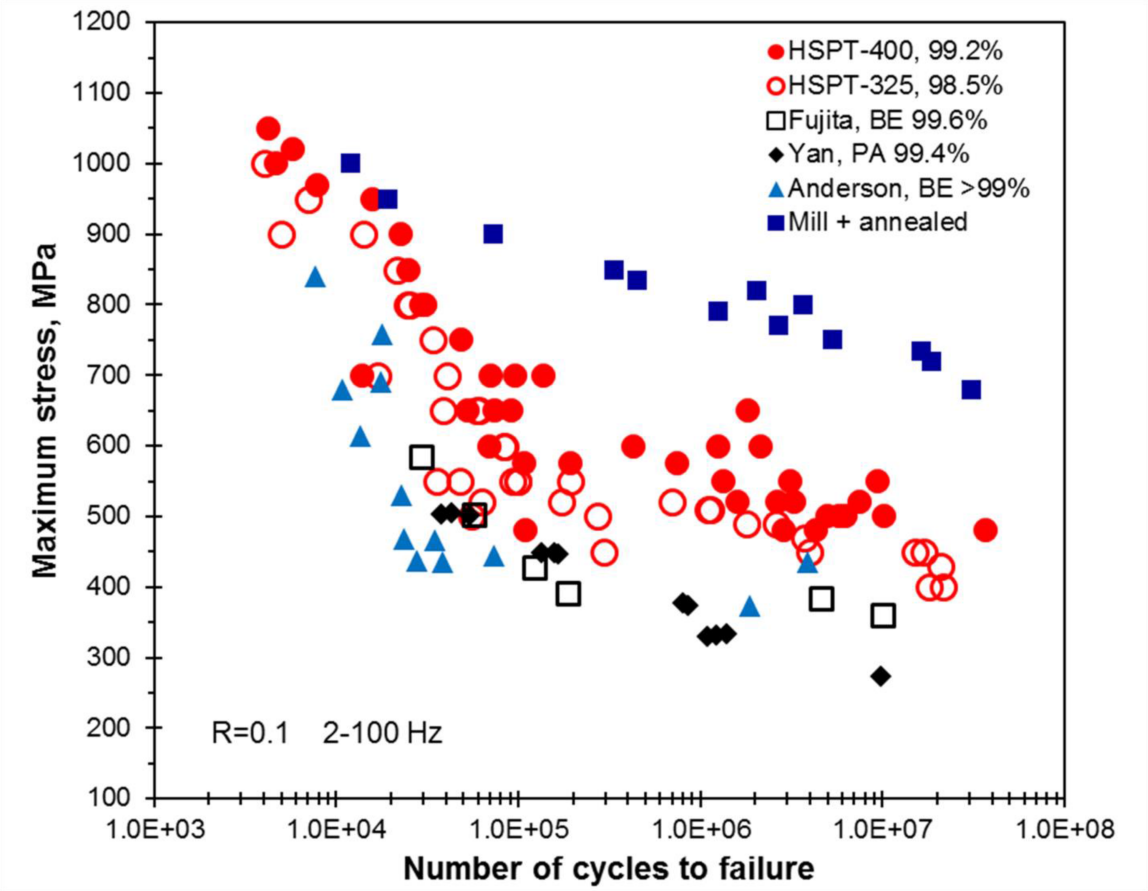

Fig. 19. Comparison of fatigue performance of HSPT samples of Ti-6Al-4V to other PM processes and also to mill annealed wrought samples.

A second set of fatigue samples were prepared to stengthen the prior data set statistically, and to provide a comparison of HSPT to vacuum sintering of Ti-6Al-4V. Figure 20 shows these two data sets compared to shaded regions highlighting the ranges of values from the literature for BE and PA PM processes, and also for mill annealed wrought samples. At ten million cycles the HSPT is approximately 150 MPa higher than the vacuum sintered material. The primary reason for the vacuum sintered samples having reduced fatigue performance is likely the coarser grain structure, particularly α grains, likely at the grain boundaries, but possibly within lamellae.

Finally, fatigue performance was also examined for the post-sintering heat treatments described above that result in bi-modal and globularized microstructures, similar to those seen in wrought materials. Figure 21 shows s-n curves for β annealed HSPT (which essentially destroys the fine grained structure formed during the HSPT process) with HSPT plus the heat treatments providing both a globularized and a bi-modal microstructure. In both of the latter cases, the HSPT samples showed fatigue performance approaching an endurance limit of approximately 600 MPa, in the upper range of wrought materials. This is an exceptional acheivement in fatigue properties, although further testing should be done for statistical accuracy.

Overall, the fatigue perfomance provided by HSPT exceeded the milestones for this project, but also pushed beyond this level and the research summarized here provides very encouraging data toward commercialization of this process. Fatigue performance has been one of

the problem areas for the wider use of PM Ti materials, and the data obtained in this project provides motivation for further refinement and industrial trials of these materials.

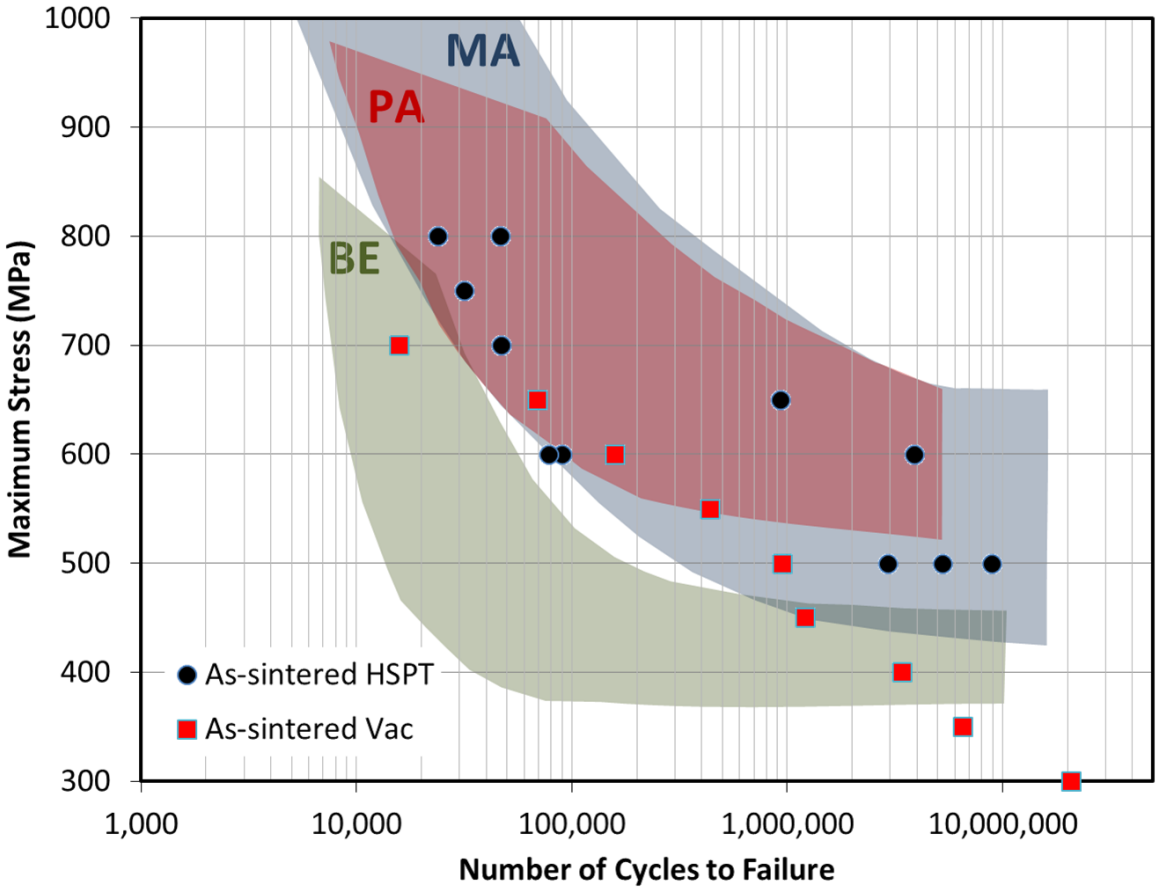

Fig. 20. The S-N curves for as-sintered Ti-6Al-4V produced via HSPT versus vacuum sintering. For reference, these data are overlaid on the fatigue life scatter-bands (prepared from data in the ASM Handbooks23) for Ti-6Al-4V produced via wrought processing with a mill-annealed microstructure (MA), pre-alloyed powder metallurgy (PA), and blended elemental powder metallurgy (BE).

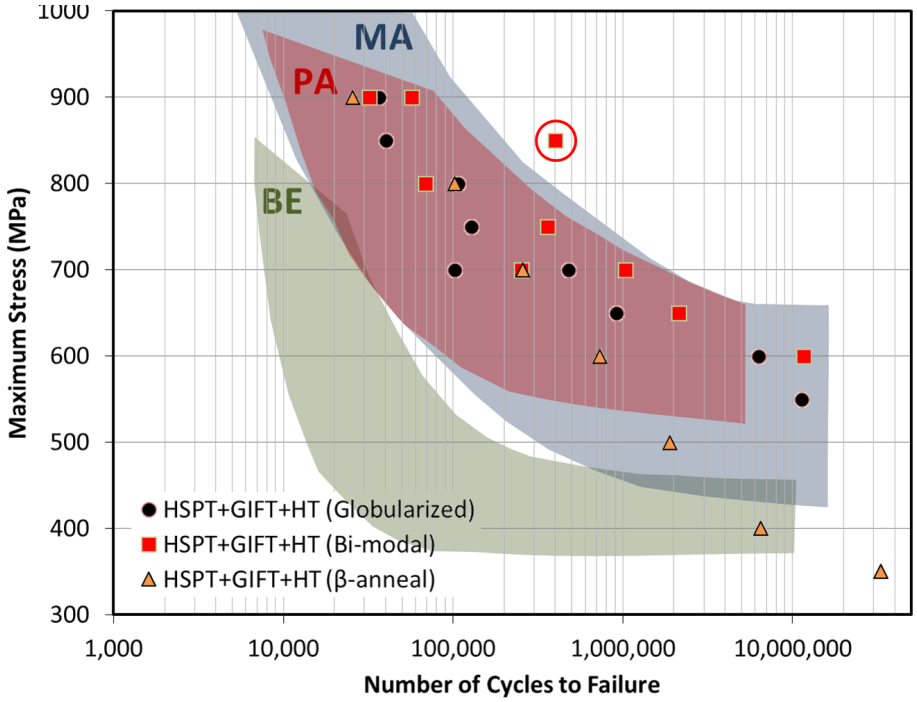

Fig. 21. S-N curves for Ti-6Al-4V produced via HSPT followed by GIFT and heat treated to produce "globularized" versus bi-modal versus β-annealed microstructures. For reference, these data are overlaid on the fatigue life scatter-bands (prepared from data in the ASM Handbooks23) for Ti-6Al-4V produced via wrought processing with a mill-annealed microstructure (MA), pre-alloyed powder metallurgy (PA), and blended elemental powder metallurgy (BE).

Benefits Assessment

Titanium is traditionally thought of as a sustainability material because of its potential for light-weighting and increasing service life of components which are traditionally made of steel. Additionally, the costs associated with the adoption of titanium in commercial and industrial applications are usually assumed to be predominately related to the extractive process. Therefore, the majority of published studies that discuss titanium with regards to sustainability focus primarily on titanium's impact on energy use in end-user applications and discuss the feasibility of such implementations relying on the reduction in cost of the extractive process (e.g. Kroll Process) [35]. However, while the energy requirements to reduce titanium to a usable metal are relatively high, the majority of the energy use and, therefore, cost associated with the production of end-user titanium products is from the often complicated, many-step, and low-yield wrought processes that are employed. In fact, it has been reported that, for some mill products, over 90% of the cost results from the forming processing required to yield the desired geometry [36]. Because of these shortcomings of studies published to date, and the salient fact that HSPT is not an extractive process, the author has endeavored to create a comparative energy model for the production of specific titanium products from sponge by traditional melt-wrought processing versus HSPT. An energy model has been chosen over cost model for two reasons. First, in a comparative model energy and cost are directly related. Second, if this or any other technology is capable of making titanium a viable replacement for steel, we will see a dramatic increase in production rates of titanium components. If this happens, the energy required to produce the components themselves will become an important environmental as well economical consideration.

In order to generate an accurate comparison between the energy efficiency of the HSPT process and a wrought process, it is necessary to identify a specific component to be produced. While complex geometries are best suited to outline the superior efficiencies of a near-net-shape process such as HSPT, a relatively simple 2" round bar stock was chosen to provide an extremely conservative comparison between HSPT and wrought processing routes.

Wrought processing of titanium is a competitive market. Consequently, actual data from the industrial processes are understandably guarded and, therefore, unavailable for this study. Additionally, HSPT has yet to be commercialized and, therefore, actual production-scale data does not exist. Therefore, for this model the we started with first principles to model the theoretical energy requirements of each known step for each process. These theoretical calculations were then adjusted using published or calculated, when necessary, efficiencies of the equipment required for each of these processes.

HSPT Energy Model

While most of the preliminary HSPT research to date achieved dehydrogenation under vacuum, it should be realized the dehydrogenation thermodynamics and kinetics are ruled purely

by the partial pressure of hydrogen and not by the total pressure of the reaction vessel. Therefore, dehydrogenation can be achieved under a protective gas at atmospheric pressure, assuming the gas has a low enough hydrogen concentration. A process that consists of cold iso-static pressing (CIP) followed by continuous multi-zone sintering was considered in order to develop a quantitative model for energy consumption.

In order to model the CIP energy requirements, it was assumed that the vast majority of energy will be required to drive the hydraulic pumps to generate the compaction pressure. In order to calculate the theoretical work required to achieve a specified change in density, one must know how the density of a compact changes as a function of applied pressure. Compaction experiments at the Army Research Laboratory have determined that the green density of TiH_2 as a function of CIP pressure adheres to the following compaction equation developed by German:

$$\rho = \rho_0 + AP^{1/3} \qquad \text{Eq. 1}$$

where ρ_o is initial density, P is the compaction pressure, A is a process dependent constant (1.518 kg m-3 Pa-1/3 for this powder), and ρ is the resulting density [38}. Using the above equation, one may calculate theoretical work performed during CIP from tap density (2.13 g/cc) to desired green density (3.2 g/cc):

$$E_{\text{compaction}} = \frac{E_{\text{compaction,theo}}}{\eta_{\text{hydraulic}}} = 3.93\ \text{kWh/ton} \qquad \text{Eq. 2}$$

Hydraulic efficiency is generally governed by frictional forces exerted on the pressure medium due to the geometry of the motors, pipelines, and pressure cells. For this model, it was assumed that this process would have a hydraulic efficiency of 75%, which is a rule-of-thumb total efficiency value commonly used for calculations of hydraulic power consumption [38]. Therefore, taking into account the hydraulic efficiency, we may calculate the actual energy required for compaction as:

$$E_{\text{compaction}} = \frac{E_{\text{compaction,theo}}}{\eta_{\text{hydraulic}}} = 3.93\ \text{kWh/ton} \qquad \text{Eq. 3}$$

It is assumed that all energy required for compaction will be supplied in the form of electricity. To determine sintering energy requirements, a continuous, fuel-fired sintering furnace with a stainless steel conveyor belt and three gas-shielded zones was modeled. The theoretical energy required for sintering titanium by this method is calculated from the energy required to heat TiH_2 to the sintering temperature (1200°C) using the heat capacity of TiH_2 (0.603 J/g-K) [39], as well as the energy required to overcome the endothermic dehydrogenation reaction.

$$E_{\text{sinter,theo}} = \int_{25℃}^{1200℃} C_{\text{p,TiH}_2}\,dT + \Delta H_{\text{TiH}_2 \rightarrow \text{Ti} + \text{H}_2} = 3682.42\,\frac{\text{kJ}}{\text{kg}} = 1022.89\ \text{kWh/ton}$$

Sintering efficiency of the system was calculated by modeling all parasitic heat flow (i.e. energy to heat stainless steel conveyor belt, energy to heat constant flow of shielding gas in each zone, and heat transfer through furnace insulation). Specific energy of the process is strongly dependent on material production rates. Therefore, for this model a single stream production rate of 220 kg/hr was chosen. In order to accommodate this production rate, it was assumed that a three zone furnace with a 314 stainless steel conveyor belt, measuring 46 cm wide by 1 cm thick, moving at a rate of 20 cm/min was loaded with an average of 4 g/cm^2 of parts to be sintered.

The next necessary determination for this calculation is the size and operating temperatures of each zone in the furnace. Using the current sintering profile for HSPT, we know that the parts must sinter at 1200°C for 4 hours, they must go through eutectoid decomposition at 750°C for 4 hours, and then must be dehydrogenated at 700°C for 8 hours. Therefore, using the belt rate of 20 cm/min and required dwell times, we are able to quickly determine the length of each zone in the furnace to be 4800 cm each for Zone 1 and Zone 2, and 9600 cm for Zone 3. Based on the belt width of 46 cm and reported dimensions for similar belt-driven furnaces [40], the proposed furnace will have an internal height of 40 cm and an internal width of 50 cm. The first energy consideration in modeling the sintering furnace is the enthalpy required to heat the parts and conveyor belt in each zone. This "ramp power" for the proposed furnace can be calculated from reported heat capacity values for TiH2 (0.603 J/g-K), Ti (0.524 J/g-K), and 314 stainless steel (SS) (0.5 J/g-K) [39,41] along with the mass flow rates of parts (μparts = 61.33 g/s) and belt (μbelt = 37.57 g/s) into each zone:

$$P_{\text{ramp}} = \int_{25℃}^{1200℃} \left(\mu_{\text{parts}} C_{\text{p,TiH}_2} + \mu_{\text{belt}} C_{\text{P,SS}}\right) dT + \int_{1200℃}^{750℃} \left(\mu_{\text{parts}} C_{\text{p,Ti}} + \mu_{\text{belt}} C_{\text{P,SS}}\right) dT + \int_{750℃}^{700℃} \left(\mu_{\text{parts}} C_{\text{p,Ti}} + \mu_{\text{belt}} C_{\text{P,SS}}\right) dT = 37.64 \text{ kW} \quad \text{Eq. 4}$$

The second energy consideration will be the power required to overcome the endothermic dehydrogenation reaction. This can be calculated from the literature-reported enthalpy of formation for TiH_2 (〖ΔH〗 _(TiH_2 → Ti + H_2)=2.97 "kJ/g") [42] and the same mass flow rate of parts used in the previous calculation:

$$P_{\text{dehydro}} = \mu_{\text{parts}} \Delta H_{\text{TiH2} \rightarrow \text{Ti} + \text{H2}} = 182.40 \text{ kW} \quad \text{Eq. 5}$$

The third energy consideration will be the power required to heat the protective gases in each zone. These gases are required to both protect the parts and control the hydrogen concentration in the parts during sintering and heat treatment. The gas will be run counter-current to the parts. This will allow the gas to be preheated by the parts as they are leaving the hotter zones and will, therefore, allow a large portion of the energy required to initially heat the parts to be reclaimed by the flowing gases. In order to prevent contamination of the zones by back diffusion of gases, a sufficient linear velocity of the flowing gas will be required. For this model, a gas velocity of 4 cm/s was chosen. Then, using the cross-sectional area of the furnace, a required flow rate of Q_{gas} = 8 L/s was calculated. Using the current sintering conditions for

HST, we know that Zone 1 and Zone 2 must be 90% Ar/10% H_2 and Zone 3 must be 100% Ar. Therefore, using the reported heat capacities for Ar (20.786 J/mol-K) and H2 (20.836 J/mol-K), the power required to heat the gases can be calculated:

$$P_{\text{gas}} = Q_{\text{gas}} \frac{1}{24.5\text{L/mol}} \left[\int_{25℃}^{700℃} C_{\text{p,Ar}} dT + \int_{700℃}^{750℃} \left(0.9C_{\text{p,Ar}} + 0.1C_{\text{p,H2}}\right) dT + \int_{750℃}^{1200℃} \left(0.9C_{\text{p,Ar}} + 0.1C_{\text{p,H2}}\right) dT \right] = 8.11 \text{ kW} \quad \text{Eq. 6}$$

The last energy consideration will be heat lost due to imperfect insulation of the furnace. This is the most subjective of the calculations, as the efficiency of the insulation can vary widely depending on the design of the furnace and selection of the insulating materials. Therefore, to make a model which is representative of a feasible industrial process, we will use a design similar to those employed in continuous belt-driven furnaces currently used in the PM industry [41]. For the proposed furnace, each zone will be insulated by high density (22 lb/ft^3 or 0.35 g/cm^3) insulating fiberboard at a thickness of t = 12 inches (30.48 cm). Based on the cross-sectional area of the furnace and the length of each zone, we know that Zones 1 and 2 will each have an internal surface area of SA = 864,000 cm^2 and Zone 3 will have a SA = 1,728,000 cm^2. Of course, the heat transfer across the insulation will vary with the internal temperature of each zone. Therefore, the following linear relationship between furnace temperature and thermal conductivity was established using thermal conductivity data from a leading manufacturer of high density refractory fiberboard [43]:

$$k \text{ (W/cm-℃)} = 1.434\times10^{-6} T(℃) + 1.971\times10^{-4} \quad \text{Eq. 7}$$

The known thermal conductivity of each zone was then used to calculate the power required to compensate for this heat loss:

$$\begin{aligned} P_{\text{insulation}} &= Q_{\text{Zone 1}} + Q_{\text{Zone 2}} + Q_{\text{Zone 3}} \\ &= \frac{k_{1200℃} SA_{\text{Zone 1}}}{t} + \frac{k_{750℃} SA_{\text{Zone 2}}}{t} + \frac{k_{700℃} SA_{\text{Zone 3}}}{t} \\ &= 139.98 \text{ kW} \end{aligned} \quad \text{Eq. 8}$$

By combining the power for each source of heat flow/loss, we may calculate the total specific energy required for the sintering process:

$$E_{\text{sinter}} = \frac{P_{\text{ramp}} + P_{\text{dehydro}} + P_{\text{gas}} + P_{\text{insulation}}}{\mu_{parts}} = 1667.27 \text{ kWh/ton} \quad \text{Eq. 9}$$

It is assumed that all energy required for sintering will come from the burning of fuel.

Wrought Process Energy Model

The most common wrought process to produce Ti-6Al-4V bar stock involves ingot formation by vacuum arc re-melting (VAR) to improve purity (most grades are achieved by either double or triple melting the material), followed by hot-working above the β-transus to produce desired geometry (2 inch round bar in this model) [44]. The theoretical energy required to VAR a double-melt ingot will be twice the enthalpy required to heat and melt titanium [42]:

$$E_{\mathrm{VAR,theo}} = 2\left(\int_{25℃}^{1670℃} C_{\mathrm{p,Ti}}\,dT + \Delta H_{\mathrm{fusion,Ti}}\right) = 2315.16\,\frac{\mathrm{kJ}}{\mathrm{kg}} \quad \text{Eq. 10}$$

$$= 643.1\ \mathrm{kWh/ton}$$

In order to calculate the electricity requirements for VAR, actual energy requirements for industrial VARs for the production and recycling of iron alloys reported in literature [45] were compared to theoretical energy requirements to heat and melt iron. From this comparison, it has been determined that VARs operate between 23.8% and 31.4% total efficiency. Therefore, a value of 33% has been chosen to give wrought processing the most optimistic evaluation for this model. Taking this efficiency into account, we may calculate the actual energy required for VAR:

$$E_{\mathrm{VAR}} = \frac{E_{VAR,\mathrm{theo}}}{\eta_{\mathrm{VAR}}} = 1948.79\ \mathrm{kWh/ton} \quad \text{Eq. 11}$$

It is assumed that all energy required for VAR will be supplied in the form of electricity.

Modeling forging is exceedingly difficult due to the myriad parameters which affect the energy consumption of the process. Therefore, in order to simplify the problem in this model, the theoretical energy requirements to heat and mechanically work the material were considered and the efficiencies reported in literature for these industrial processes were applied. For this model, a standard 28 inch (71.12 cm) diameter, 3,400 kg, 769,231 cm3, double-melt ingot was assumed to be the forge feedstock to produce 2 inch (5.08 cm) diameter round bar stock by gyratory forging machines (GFM). The theoretical mechanical work required to effect this geometric change at the forging pressure for titanium of 200MPa [44] is:

$$E_{\mathrm{forge,mech,theo}} = \int_{r_i}^{r_f} F\,dr = \int_{r_i}^{r_f} \frac{2PV}{r}\,dr = 2PV\ln\left(\frac{r_f}{r_i}\right) = 238.83\,\frac{\mathrm{kJ}}{\mathrm{kg}} \quad \text{Eq. 12}$$

$$= 66.34\ \mathrm{kWh/ton}$$

It may be assumed that the GFM's are hydraulic. Therefore, taking into account the rule-of-thumb hydraulic efficiency of 75%, we may calculate the actual mechanical work required for forging:

$$E_{\text{forge,mech}} = \frac{E_{\text{forge,mech,theo}}}{\eta_{\text{hydraulic}}} = 88.46\ \text{kWh/ton} \quad \text{Eq. 13}$$

It is assumed that all energy required for the mechanical work will supplied in the form of electricity.

The theoretical energy required to maintain the required forging temperature (900 °C) [44] is the sum of the initial energy to heat the material from room temperature and the energy required to reheat the material after each pass. It has been assumed that the material will cool approximately 200°C between passes. Assuming the volume of the ingot remains constant, we may calculate the initial and final lengths to be 193.6 cm and 379.5 m, respectively. If an elongation of 100% for each pass is assumed, this forging process will require 8 passes. Therefore, the theoretical energy to heat the titanium to the appropriate forging temperature is:

$$E_{\text{forge,heat,theo}} = \int_{25℃}^{900℃} C_{\text{p,Ti}}dT + 8\int_{700℃}^{900℃} C_{\text{p,Ti}}dT = 1296.9\frac{\text{kJ}}{\text{kg}} = 360.25\ \text{kWh/ton} \quad \text{Eq. 14}$$

Forge furnaces are reported to operate at 20~60% efficiency [46]. Therefore, for this model, it has been assumed the forging furnaces operate at 60%. Taking this efficiency into consideration, we may calculate the actual energy required to heat the material during forging:

$$E_{\text{forge,heat}} = \frac{E_{\text{forge,heat,theo}}}{\eta_{\text{furnace}}} = 600.42\ \text{kWh/ton} \quad \text{Eq. 15}$$

It is assumed that all energy required for heating will come from the burning of fuel.

Traditional titanium forging operations tend to have low yields due to oxide formation and removal [35]. Therefore, a material yield for the forging step of 75% has been considered in the calculation. It should be noted that the removal of the oxide layer is usually performed between forging passes, which would result in greatly increased cooling and reheating energy requirements. However, this consideration has been omitted in the model to maintain an optimistic evaluation of wrought processing.

Energy Model Comparison

Table IV gives the energy requirement comparison for the two processes when process efficiencies are ignored. This comparison is useful from a standpoint that additional engineering optimizations are always possible for any process, though the thermodynamics of the desired reactions are an insuperable lower boundary for specific energy consumption.

Table IV. Theoretical minimum energy requirements of modeled processes.

HSPT	kWh/ton	Wrought	kWh/ton
Compaction	2.95	VAR	643.10
Sintering	1022.89	Forging	426.59
Total	**1025.84**	**Total**	**1069.69**

Conversely, Table V gives the energy requirement comparison for the two processes accounting for efficiency of each step in each process. As mentioned above, the efficiency of HSPT sintering was determined by modeling heat flow of the entire sintering process, whereas the remaining process efficiencies (CIP/forge hydraulics, VAR furnace, and forge furnace) were assumed to be consistent with values reported in literature.

Table V. Calculated energy consumption and equivalent coal consumption for modeled processes.

HST	Electricity (kWh/ton)	Fuel (kWh/ton)
Compaction (kWh/ton)	3.93	0.00
Compaction Yield	100%	100%
Sintering (kWh/ton)	0.00	1667.27
Sintering Yield	100%	100%
Total Energy	3.93	1667.27
Equivalent Coal (ton Coal per ton Ti)	1.97E-03	0.27
Total Equivalent Coal (ton/ton)	**0.27**	
Wrought	**Electricity (kWh/ton)**	**Fuel (kWh/ton)**
VAR (kWh/ton)	1948.79	0.00
VAR Yield	100%	100%
Forging (kWh/ton)	88.46	600.42
Forging Yield	75%	75%
Total Energy	2716.32	800.56
Equivalent Coal (ton Coal per ton Ti)	1.36	0.13
Total Equivalent Coal (ton/ton)	**1.49**	

Coal energy equivalence was included in Table V to highlight the difference between thermal energy and electrical energy from fossil fuels with regard to environmental implications. In the United States, the majority of electricity is produced by burning coal [47], which only provides 2000 kWh/ton when converted into electricity, versus 6150 kWh/ton when used for thermal energy. Therefore, taking this phenomenon into consideration is important when considering fossil fuel consumption and greenhouse gas (GHG) emissions. The equivalency could have also been calculated with regard to natural gas or oil volumes with the same result, as power plants all tend to convert fuel thermal energy to electrical energy at approximately a 3:1 ratio, regardless of fuel [47]. It should also be noted that great care was taken to provide a very optimistic evaluation of traditional wrought processing. Furthermore, the model above assumes that both processes produce 2 inch round bar stock, a geometry that does not take into account the massive energy and cost savings of producing near-net-shape parts. Even with this bias towards wrought within the model, the results are clear that the HSPT process is significantly less energy intensive. Based on this model, wrought processing is nearly identical to HSPT on a purely theoretical level. However, when equipment efficiency, process yields, and electrical generation form fossil fuels are considered, wrought processing becomes 5.5 times as energy/fuel intensive.

Potential Economoic and Environmental Impact of HSPT Process

While the current project does not affect energy production, it stands to benefit energy savings in two regards. First, there is potential for significantly reducing the energy of component production and waste of Ti material (and, therefore the energy required to process that wasted portion of Ti) compared to current forging technology. The HSPT process is being compared to forging, rather than vacuum sintering technology, since the goal is to attain mechanical properties comparable or exceeding forging, a goal not attained by vacuum sintering technology. The second aspect of energy savings would result from light weighting of vehicles, equating in gasoline and diesel fuel savings over the entire US fleet and beyond. All analyses below are restricted to the US economy.

The USGS reported Ti consumption in 2012 at approximately 33,000 metric tons consumed, primarily in the aerospace industry, but with significant useage by medical and marine applications, as well as in armor, power generation and sporting goods (U.S. Geological Survey, Mineral Commodity Summaries, January 2013). The average price in 2012 for Ti sponge was $11.75/kg. Establishing projections for Ti usage and price in 2020 is likely to have significant error, but an estimate based on past usage and trends may have utility. In 2006 TIMET showed an increase across industrial use of Ti of approximately 33% over the preceding decade, and a more modest 13% in aerospace applications. Given a general slowing of the world ecconomy, we will assume a 10% increase in Ti metal use in the US by 2020 from 2012 figures, or approximately 36,300 metric tons/year.

Table V, above, presents data from a model of comparative energy costs between the HSPT process and forging, based on a number of assumptions, but many of which favor the perspective of wrought technology in order to obtain a conservative appraisal of potential energy savings. Here we estimate 35,000 kWh/ton_{Ti} of total energy for the wrought process, and a process savings of approximately 82% for HSPT over wrought materials. The projected total energy cost for Ti component production in the US in 2020 using the wrought process would thus be 1,270.5 million kWh, or approximately 4.3 Tbtu. So, assuming all component production shifted to HSPT from forging technology (this is unlikely for both technological and other reasons), the savings would be 3.5 Tbtu. Generally, the intransigence of industry to change feedstock or process is balanced by competetiveness in the marketplace. Estimating the percentage of total market conversion from wrought to HSPT processing is beyond the expertise of our team, but given only five years between project completion and the year 2020, half the market would probably be an optimistic estimate, at approximately 1.75 Tbtu/year in savings.

Considering all energy in the process as kWh for simplicity, and taking an average of 15 cents per kWh, gives an annual savings of approximately $95 million per year. The change with 50% market conversion would result in 22,143 metric tons of coal per year, or 63,329 metric tons of CO_2 (using a factor of 2.86 for CO_2 to coal from EPA).

The second area of energy savings would come via the light weighting of vehicles, resulting in savings of gasoline and diesel fuel. The primary target component for this project within the drive train for automobiles is the connecting rod, and an example PM steel connecting rod was measured in our lab at 615 g. An additonal component that would potentially shift from steel to Ti, given a decrease in energy and cost for Ti component processing, is the exhaust

system. This is particularly likely given the corrosion resistance of Ti, which would extend the service life of the exhaust system, and given the lower mechanical property requirements for exhaust systems compared to drive train components. The third and final components for this initial analysis are the suspension springs. All of these parts are currently steel or stainless steel in commercial automobiles. The weight savings by switching to Ti parts for connecting rods, exhaust system and suspension springs for a 4-cylinder vehicle are estimated to be 0.56 kg, 2.6 kg and 2.4 kg, respecitvely, for a total of 5.56 kg. Assuming an average vehicle mass of 1,300 kg, this represents a 0.43% reduction in mass for an average vehicle. Since a 1% reduction in mass equates to a 0.7% increase in fuel efficiency (Nippon Steel Techinical Report #85, January, 2002), this gives a 0.3% increase in average fuel efficiency. Although this may seem a modest improvement, it should be considered that many other steel components of the vehicle may also be candidates for replacement by Ti parts, and that the extrapolation of this figure across the majority of vehicles in the US will result in significant savings.

In 2009 the US Dept. of Tansportation reported there were slightly over 254 million registered vehicles, and in 2010 an average light duty vehicle fuel efficiency of 23.5 mpg (10 km/l). This gives an estimated savings in fuel of 486 million gallons per year (1,839 million liters/year). The average cost of gasoline in the US on April 8, 2013 was 3.6 $/gal (0.95$/l), yielding a savings of approximately 1.75 billion dollars per year.

The EPA estimates 4.8 metric tons of CO_2 per vehicle in the US, so a 0.3 % increase in fuel efficiency equates to 3.6 million metric tons of CO_2 per year. Even though there is only a small decrease in mass of a single vehicle, the reduction in CO_2 from light weighting dwarfs the savings on the Ti component production side. That said, with increased use of Ti and decreased cost, the environmental savings from production could be more profound, increasing in a linear function with production.

Commercialization

With movement of the project into its third year, emphasis was placed on commercialization. In addition to interest from Tier One auto parts suppliers, Reading Alloys entered into discussions and negotiations with the University of Utah's Technology & Venture Commercialization Office and signed an option for licensing of the technology in spring of 2015. Markets and products outside the limited licensing agreement signed by Reading Alloys with the University of Utah are ongoing, and the team intends to find other potential licensees over the coming year.

Public releases of the successes in mechanical properties achieved during the project and the reduced production costs of the process have been submitted to DOE and to trade publications, and a slide deck was prepared for DOE for potentially interested industrial contacts. Information on the technology was also made available to the University of Utah's Office of Technology & Venture Commercialization, which leads such endeavors in collaboration with the PI on behalf of the university.

Accomplishments

Peer Reviewed Journal Articles

F. Cao, K.R. Chandran, P. Kumar, P. Sun, Z.Z. Fang & M. Koopman, "New Powder Metallurgical Approach to Achieve High Fatigue Strength in Ti-6Al-4V Alloy." *Metallurgical and Materials Transactions A*, *4 (2016) 7*(5), 2335-2345.

P. Kumar, K.R. Chandran, F. Cao, M. Koopman & Z.Z. Fang, "The Nature of Tensile Ductility as Controlled by Extreme-Sized Pores in Powder Metallurgy Ti-6Al-4V Alloy," *Metallurgical and Materials Transactions A*, (2016) *47*(5), 2150-2161.

P. Sun, Z. Z. Fang, M. Koopman, Y Xia, J. Paramore, K. Chandran, Y. Ren and J Lu, "Phase Transformations and Formation of Ultra-Fine Microstructure During Hydrogen Sintering and Phase Transformation (HSPT) Processing of Ti-6Al-4V," **Metallurgical and Materials Transactions A**, (2015) in press, but available at: http://link.springer.com/article/10.1007/s11661-015-3141-8/fulltext.html

J. D. Paramore, Z. Z. Fang, P. Sun, M. Koopman, K.S. Ravi Chandran, and M. Dunstan, "High Performance Ti-6Al-4V with Wrought-like Microstructures and Mechanical Properties via Hydrogen Sintering and Phase Transformation (HSPT)," **Scripta Materiala**, 107 (2015) 103-6.

F. Cao, P. Kumar, M. Koopman, L. Chenluh, Z.Z. Fang, and K.S. Ravi Chandran. "Understanding competing fatigue mechanisms in powder metallurgy Ti–6Al–4V alloy: Role of crack initiation and duality of fatigue response." **Materials Science and Engineering: A** 630 (2015) 139-145.

P. Sun, Z. Z. Fang, M. Koopman, J. Paramore, K. S. R. Chandran,
Y. Ren and J. Lu, "An experimental study of the (Ti–6Al–4V)–xH phase diagram using in situ synchrotron XRD and TGA/DSC techniques." **Acta Materialia** 84 (2015): 29-41.

P. Sun, Z.Z. Fang and M. Koopman, "A Comparison of Hydrogen Sintering and Phase Transformation (HSPT) Processing with Vacuum Sintering of CP-Ti," **Advanced Engineering Materials**, 15 (2013) 1007-1013.

Conference Proceedings

Pei Sun, Z. Zak Fang, Mark Koopman, James Paramore and KS Ravi Chandran, An Investigation of Phase Transformation in (Ti-6Al-4V)-H Using In-situ High-energy Synchrotron XRD, Proc. Ti-2015: The 13th World Conference on Ti, August 16-20, 2015, San Diego, CA, USA.

Pankaj Kumar, KS Ravi Chandran, F. Cao, Pei Sun, Mark Koopman and Z. Zak Fang, Effect of Powder Processing and Sintering on Tensile Ductility of PM Ti-6Al-4V Alloy Made by Hydrogen Sintering of Titanium Hydride Powders, Proc. Ti-2015: The 13th World Conference on Ti, August 16-20, 2015, San Diego, CA, USA.

Fei Cao, KS Ravi Chandran, Pankaj Kumar, Pei Sun, Mark Koopman and Z. Zak Fang, Improved Fatigue Performance of PM Ti-6Al-4V Alloy Processed by Hydrogen Sintering and Phase Transformation of TiH_2, Proc. Ti-2015: The 13th World Conference on Ti, August 16-20, 2015, San Diego, CA, USA.

M.Dunstan, J. Paramore, M. Koopman, Z.Z. Fang, HSPT: A Low-Cost Method for Producing Titanium Alloys with Exceptional Mechanical Properties, Advances in Powder Metallurgy & Particulate Materials, Proceedings of the Powder Metallurgy World Congress - 2014.

L. Yang, P. Sun, M. Koopman, Z.Z. Fang, Effects of Ball Milling and Sintering Processing on Oxygen Content in PM Titanium, Advances in Powder Metallurgy & Particulate Materials, Proceedings of the Powder Metallurgy World Congress - 2014.

Patent Application

Fang, Zhigang Zak, Pei Sun, James Paramore, Hongtao Wang, Mark Koopman, and Lu Yang. "Powder metallurgy methods for the production of fine and ultrafine grain ti and ti alloys." U.S. Patent Application 14/152,787, filed January 10, 2014.

Student Dissertations and Theses

James Paramore, Relationship between Processing, Structure, and Properties of Titanium Alloys Produced by Hydrogen Sintering and Phase Transformation (HSPT), PhD dissertation, University of Utah, 2015.

Pei Sun, PhD dissertation, Powder Metallurgy Titanium by the Hyrdorogen Sintering and Phase Trnasformation (HSPT) Process, University of Utah, 2015.

Lu Yang, Effect of Particle Size on Oxygen Content and Porosity of Sintered Ti-6Al-4V, Masters Thesis, University of Utah, 2015.

Conclusions

- The hydorgen sintering and phase transformation (HSPT) process is a cost effective alternative to wrought processing for many industrial applications.
- Replacement of steel components in automobiles and other vehicles would result in significant reduction in fossil fuel use, and consequently in CO_2 production.
- Milling experiments in protective environments, such as light and heavy mineral oils, showed reduced oxygen contents compared to conventional milling in heptane or inert atmospheres. This result may lead to improved milling procedures that can assist in minimizing oxygen content in final samples, and therefore, in superior mechanical properties in a range o foxygen sensitive PM materials.
- Results of this project in determining relevant sections of the (Ti-6Al-4V)-H phase diagram, principally by *in situ* synchrotron experiments, have provided valuable imformation on the phase transformations in this system, drastically modifying the prior phase diagrams in this material system. These data are relevant not only to HSPT, but also to thermal hydrogen processing and to hydride-deydride powder processes.
- Due to the refined grain sturcture of HSPT over vacuum sintering, the tensile properties of HSPT are superior to all other PM technologies, including vacuum sintering, showing ultimate tensile strength exceeding 1,000 MPa while maintatining good ductility. The tensile strength of HSPT samples actually exceeds that of wrought materials tested.
- Heat treatments commonly used in wrought materials, processes which do not add inordeinate costs to the HSPT process, yield beneficial microstructures that have not previously been seen in other PM Ti materials.
- Fatigue properties from the HSPT process showed improved performance over all but the most energy intensive and costly PA methods in the as-sintered state. With the addition of PIF and/or simple post-sintering heat treatments, the fatigue performance of HSPT materials was shown to exceed all other PM processes and to be competetive with wrought processing.

Recommendations

Primarily due to the inherent properties of titanium, particularly its high specific mechanical properties and excellent corrosion resistance, further work in titanium processing should be pursued. Further efforts should be applied to stimulate research and commercialization of Ti processes that reduce the cost of this invaluable material, in order to take full advantage of preoperties with the potential to reduce long range energy utilization and enhance sustainable engineering design.

The HSPT process has shown exceptional mechanical properties, comparable to those of the much more expensive wrought processing technologies that predominate the current marketplace. Comparative cost analysis has indicated that commercializtion of this technology could significantly reduce the cost of producing small to moderate size components by a blended element powder metallurgy approach. Programs that seek to link the fundamental mechanical properties already demonstrated to actual component testing and applications should be sought, either through government assisted programs or through privatelty funded industrial development.

References

[1] C. Leyens and M. Peters, *Titanium and Titanium Alloys*: John Wiley & Sons, 2006.

[2] D. Eylon and F. H. Froes, "Titanium P/M Products," in *ASM handbook, Vol. 02: Properties and Selection: Nonferrous Alloys and Special-Purpose Materials*. vol. 02, J. R. Davis, P. Allen, S. R. Lampman, T. B. Zorc, S. D. Henry, J. L. Daquila*, et al.*, Eds., ed Materials Park, Ohio: ASM International, 1990.

[3] M. Qian, "Cold compaction and sintering of titanium and its alloys for near-net-shape or preform fabrication," *International Journal of Powder Metallurgy* vol. 46, pp. 29-44, 2010.

[4] H. Wang, Z. Z. Fang, and P. Sun, "A critical review of mechanical properties of powder metallurgy titanium," *International Journal of Powder Metallurgy,* vol. 46, pp. 45-57, 2010.

[5] Z. Z. Fang and P. Sun, "Pathways to optimize performance/cost ratio of powder metallurgy titanium - A perspective," in *1st International Conference on Powder Processing, Consolidation and Metallurgy of Titanium, December 4, 2011 - December 7, 2011*, Brisbane, QLD, Australia, 2012, pp. 15-23.

[6] Y. Yamamoto, J. O. Kiggans, M. B. Clark, S. D. Nunn, A. S. Sabau, and W. H. Peter, "Consolidation Process in Near Net Shape Manufacturing of Armstrong CP-Ti/Ti-6AI-4V Powders," *Key Engineering Materials,* vol. 436, pp. 103-11, 2010.

[7] C. G. McCracken, C. Motchenbacher, and D. P. Barbis, "Review of titaniumpowder-production methods," *International Journal of Powder Metallurgy* vol. 46, pp. 19-26, 2010.

[8] U. Zwicker, Stierstadt, and H. W. Scheicher, "Process for improving the workability of titanium alloys," United States Patent 2, 892, 742, 1959.

[9] W. R. Kerr, P. R. Smith, M. E. Rosenblum, F. J. Gurney, Y. R. Mahajan, and L. R. Bidwell, "Hydrogen as an Alloying Element in Titanium (Hydrovac)," in *Titanium '80, Science and Technology, Proceedings of the 4th International Conference on Titanium.*, Kyoto, Jpn, 1980, pp. 2477-2248.

[10] F. H. Froes, O. N. Senkov, and J. I. Qazi, "Hydrogen as a temporary alloying element in titanium alloys: thermohydrogen processing," *International Materials Reviews,* vol. 49, pp. 227-245, 2004.

[11] W. Kerr, "The effect of hydrogen as a temporary alloying element on the microstructure and tensile properties of Ti-6Al-4V," *Metallurgical and Materials Transactions A,* vol. 16, pp. 1077-1087, 1985.

[12] O. M. Ivasishin, D. G. Savvakin, F. Froes, V. C. Mokson, and K. A. Bondareva, "Synthesis of alloy Ti-6Al-4V with low residual porosity by a powder metallurgy method," *Powder Metallurgy and Metal Ceramics,* vol. 41, pp. 382-90, 07/ 2002.

[13] O. M. Ivasishin, D. G. Savvakin, V. S. Moxson, K. A. Bondareval, and F. H. S. Froes, "Titanium powder metallurgy for automotive components," *Materials Technology,* vol. 17, pp. 20-25, 2002.

[14] O. M. Ivasishin, K. A. Bondareva, V. I. Bondarchuk, O. N. Gerasimchuk, D. G. Savvakin, and B. A. Gryaznov, "Fatigue Resistance of Powder Metallurgy Ti–6Al–4V Alloy," *Strength of Materials,* vol. 36, pp. 225-230, 2004.

[15] O. M. Ivasishin, D. G. Savvakin, V. S. Moxson, K. A. Bondareva, and F. H. Froes, "High Intergrity, Low Cost Titanium Powder metallurgy Components," presented at the TMS 2002 Annual Meeting, Seattle, Washington, 2002.

[16] J. Greenspan, F. J. Rizzitano, and E. Scala, "Titanium powder metallurgy by decomposition sintering of the hydride " presented at the Titanium Science and Technology: Proceddings of the Second Internatinal Conference, Cambridge, Massachusetts, 1973.

[17] O. M. Ivasishin and D. G. Savvakin, "The impact of diffusion on synthesis of high-strength titanium alloys from elemental powder blends," in *TMS 2010 Spring Symposium on Cost-Affordable Titanium III, February 14, 2010 - February 18, 2010*, Seattle, WA, United states, 2010, pp. 113-121.

[18] O. M. Ivasishin, D. G. Savvakin, M. M. Gumenyak, and O. B. Bondarchuk, "Role of surface contamination in titanium PM," in *1st International Conference on Powder Processing, Consolidation and Metallurgy of Titanium, December 4, 2011 - December 7, 2011*, Brisbane, QLD, Australia, 2012, pp. 121-132.

[19] H. Wang, M. Lefler, Z. Z. Fang, T. Lei, S. Fang, J. Zhang*, et al.*, "Titanium and titanium alloy via sintering of TiH2," *Key Engineering Materials,* vol. 436, pp. 157-63, 2010.

[20] Z. Z. Fang, P. Sun, and H. Wang, "Hydrogen Sintering of Titanium to Produce High Density Fine Grain Titanium Alloys," *Advanced Engineering Materials,* vol. 14, pp. 383-387, 2012.

[21] M. Wasz, F. Brotzen, R. McLellan, A. Griffin, International materials reviews, 41 (1996) 1-12.

[22] L. Bolzoni, E.M. Ruiz-Navas, E. Neubauer, E. Gordo, Materials Chemistry and Physics, 131 (2012) 672-679.

[23] Y. Liu, L. Chen, H. Tang, C.T. Liu, B. Liu, B. Huang, Materials Science and Engineering: A, 418 (2006) 25-35.

[24] O.M. Ivasishin, D.G. Savvakin, M.M. Gumenyak, O.B. Bondarchuk, Key Engineering Materials, 520 (2012) 121-132.

[25] M. Yan, Y. Liu, Y. Liu, C. Kong, G. Schaffer, M. Qian, Scripta Materialia, 67 (2012) 491-494.

[26] W.H. Peter, Y. Yamamoto, W. Chen, R.R. Dehoff, S.D. Nunn, A.S. Sabau, J. Kiggans, T.R. Muth, G. Daehn, C. Tallman, Oak Ridge National Laboratory (ORNL); Shared Research Equipment Collaborative Research Center, 2013.

[27] L.R. de Andrade, E.T. Galvani, V.A.R. Henriques, S.L.G. Petroni, SAE Technical Paper, 2012.

[28] E. Baril, L. Lefebvre, Y. Thomas, Powder Metallurgy, 54 (2011) 183-186.

[29] P. Sun, Z. Z. Fang, M. Koopman, J. Paramore, K. S. R. Chandran, Y. Ren and J. Lu, "An experimental study of the (Ti–6Al–4V)–xH phase diagram using in situ synchrotron XRD and TGA/DSC techniques." Acta Materialia 84 (2015): 29-41.

[30] P. Sun, Z. Z. Fang, M. Koopman, Y Xia, J. Paramore, K. Chandran, Y. Ren and J Lu, "Phase Transformations and Formation of Ultra-Fine Microstructure During Hydrogen Sintering and Phase Transformation (HSPT) Processing of Ti-6Al-4V," **Metallurgical and Materials Transactions A**, (2015) in press, but available at: http://link.springer.com/article/10.1007/s11661-015-3141-8/fulltext.html

[31] Z.Z. Fang and P. Sun: *Key Eng. Mater.*, 2012, vol. 520, pp. 15-23.

[32] M. Hagiwara, and S. Emura: *Mater. Sci. Eng. A*, 2003, vol. 352, pp. 85-92.

[33] M. Hagiwara, Y. Kaieda, Y. Kawabe, and S. Miura: *ISIJ Int.*, 1991, vol. 31, pp. 922-90.

[34] D. Eylon: *Metall. Trans. A*, 1979, vol. 10, pp. 311-17.

[36] F. H. Froes, "Developments in Titanium P/M," [Online]. Available: http://ww.webs1.uidaho.edu/imap/MPR%20Paper.pdf.

[37] R. M. German, Powder Metallurgy Science, Princeton, New Jersey: MPIF, 1994.

[38] A. Akers and M. Gassman, Hydraulic Power Systems Analysis, New York: Taylor and Francis, 2006.

[39] M. W. Chase Jr., NIST-JANAF Thermochemical Tables, Woodbury, NY: American Chemical Society, 1998.

[40] H. Nandi, M. Thomason and M. Delhunty, "Software tool optimizes furnace design and operation," *Heat Treating Progress (USA),* vol. 2, no. 8, pp. 17-21, 2002.

[41] W. M. Haynes and D. R. Lide, CRC Handbook of Chemistry and Phyiscs, 92nd ed., Boca Raton, FL: CRC Press, 2011-2012.

[42] J. Zhao, H. Ding, X. Tian, W. Zhao and H. Hou, "Thermodynamic Calculation on the Formation of Titanium Hydride," *Chinese Journal of Chemical Physics,* vol. 21, p. 569, 2008.

[43] M. J. Donachie, Titanium: A Technical Guide, Materials Park, OH: ASM International, 2000.

[44] H. J. Mueller-Aue, "Analysis of Operation Data of Vacuum Arc and Electroslag Remelting Plant," *Journal of Vacuum Science and Technology,* vol. 8, pp. VM19-VM23, 1971.

[45] TIMET, [Online]. Available: http://www.timet.com/ingotmain.html.

[46] A. C. Thekdi, *Energy Efficiency Improvement Opportunities in Process Heating for the Forging Industry,* Canton, OH: presented at the Forging Industry Energy Workshop, 2010.

[47] U.S. Energy Information Administration, [Online]. Available: http://www.eia.gov/aer.

Appendix A

Testing Procedure and Evaluation of Fatigue Strength

Task III. Evaluation of Fatigue Properties of HSPT PM Ti-6Al-4V alloy

I. Testing Standard Followed

ASTM E466–07, "Standard Practice for Conducting Force Controlled Constant Amplitude Axial Fatigue Tests of Metallic Material." This practice covers the procedure for the performance of axial force controlled fatigue tests to obtain the fatigue strength of metallic materials in the fatigue regime where the strains are predominately elastic, both upon initial loading and throughout the test. All the tests for this project generally follow the procedures outlined in this standard.

II. Machining of Specimens

The dimension of the HSPT PM sintered blanks (typically 10 in a batch) are approximately 0.57" in dia. and 3.5" in length. From these, fatigue samples with gage sections of 0.25" dia. and 0.5" in length were machined by Westmoreland mechanical Testing & Research, Inc. The finished Gage section has a surface finish of 16 micro-inches.

III. Method of Surface Preparation

The as-machined specimens were mounted on a rotating spindle. The gage sections of the specimens were then mechanically polished with the samples rotating at about 60 rpm. The polishing started with 1200 grit SiC abrasive paper and was followed by 1 μm alumina suspension. The final polished specimens had a mirror-like finish with no visible scratches on the surface.

IV. Checks on Dimensions

The gage section diameters were measured at three locations and the average of these were used to calculate the gage section area.

V. Fatigue Testing

Fatigue test is performed on a MTS system with Flex Test 40 digital controller in load- control mode. Sine wave loading with a frequency of 35 Hz was applied to the samples. The cycling was performed in a closed-loop mode with a force sensitivity of 50 N and a tolerance of 500 N. Maximum and minimum loads exceeding the tolerance will shut down the testing.

VI. Determination of Fatigue Strength and Criterion

Fatigue strength is defined as the minimum stress level below which no specimen failure after a prescribed number of cycles. The common definition of fatigue strength or alternatively the endurance limit is the maximum stress of a fatigue cycle that runs the specimen without failure for 10 million cycles. All the tests for the project will use this criterion as a definition of fatigue strength and endurance limit.

VI. Comparison with Fatigue Strength of Wrought Ti-6Al-4V

There is no specification for fatigue strength of the commercially produced wrought material. Because processing methods, heat treatment and surface preparation of specimens all affect the fatigue strength, a range is generally quoted. As quoted by Carpenter Technology Corporation, the fatigue strength of a standard annealed Ti-6Al-4V Grade 5 Alloy will have a variation in fatigue strength as follows.

High Cycle Fatigue Strength[1]	400-700 MPa (at a stress ratio, R=0.1)

[1] Fatigue strength as quoted in Ti-6Al-4V Alloy Data Sheet, Carpenter Technology Corporation. Fatigue strength is defined as the maximum stress of the constant amplitude fatigue cycling at which the specimen does not fail in 10 million cycles.